https://ntrs.nasa.gov/search.jsp?R=19930009206 2020-03-17T07:39:13+00:00Z

IN-02
145552
P.63

NASA
Technical
Paper
3258

February 1993

Wind-Tunnel Free-Flight Investigation of a Supersonic Persistence Fighter

David E. Hahne,
Thomas R. Wendel,
and Joseph R. Boland

(NASA-TP-3258) WIND-TUNNEL FREE-FLIGHT INVESTIGATION OF A SUPERSONIC PERSISTENCE FIGHTER (NASA) 63 p

N93-18395

Unclas

H1/02 0145552

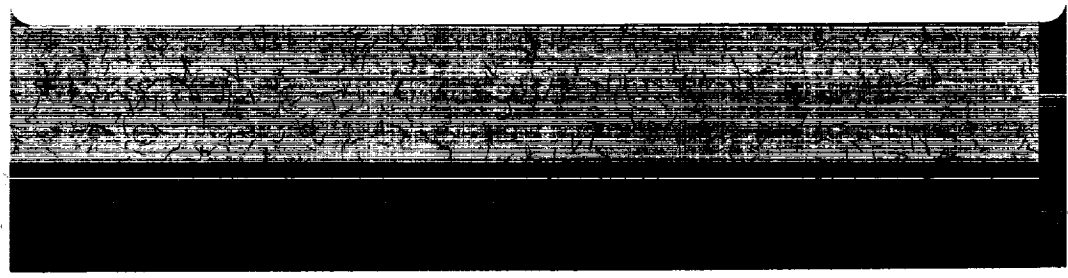

NASA

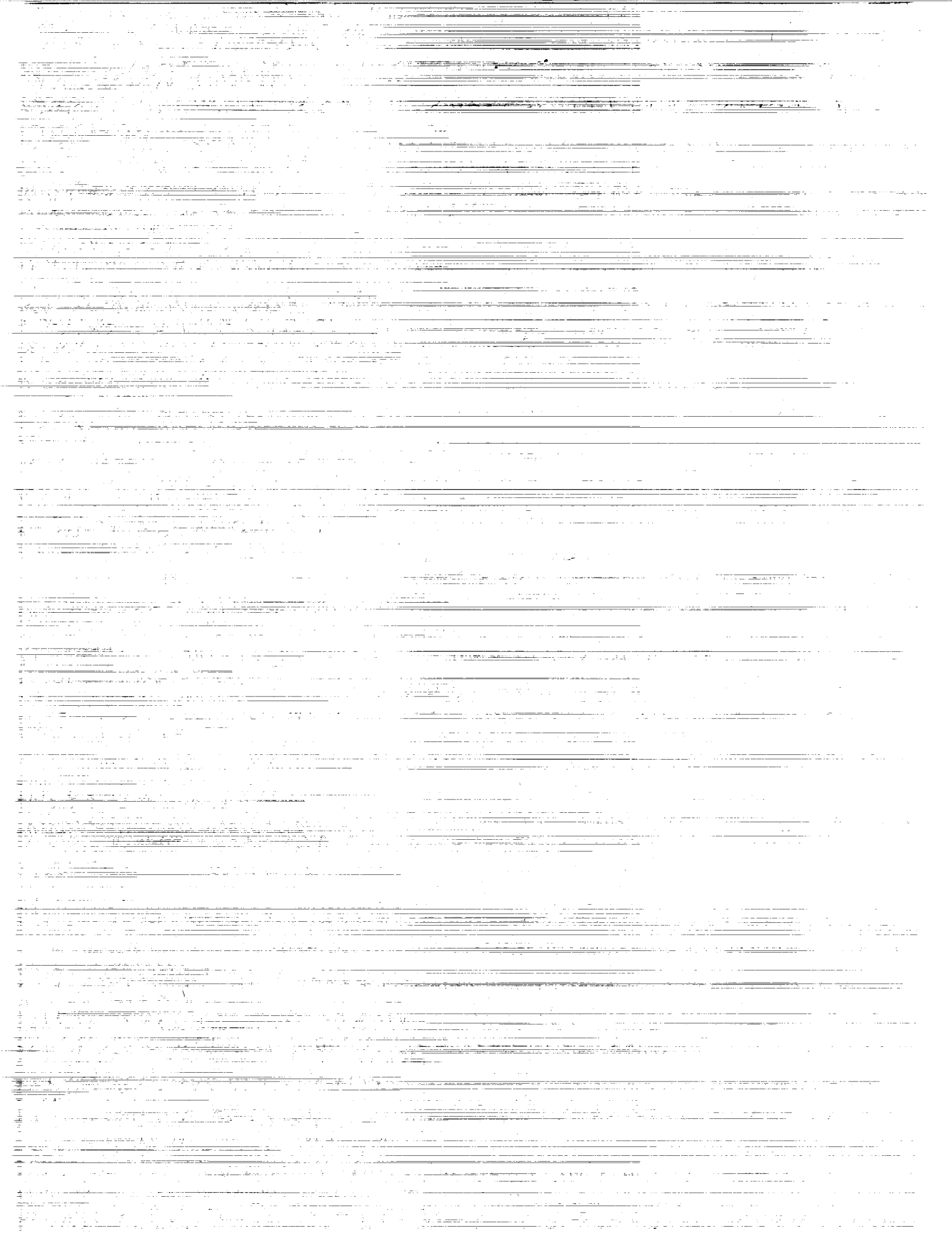

NASA Technical Paper 3258

1993

Wind-Tunnel Free-Flight Investigation of a Supersonic Persistence Fighter

David E. Hahne
Langley Research Center
Hampton, Virginia

Thomas R. Wendel
and Joseph R. Boland
McDonnell Aircraft Company
St. Louis, Missouri

NASA
National Aeronautics and Space Administration
Office of Management
Scientific and Technical Information Program

The use of trademarks or names of manufacturers in this report is for accurate reporting and does not constitute an official endorsement, either expressed or implied, of such products or manufacturers by the National Aeronautics and Space Administration.

Summary

Wind-tunnel free-flight tests were conducted in the Langley 30- by 60-Foot Tunnel to examine the high-angle-of-attack stability and control characteristics and control law design of a supersonic persistence fighter (SSPF) at $1g$ flight conditions. The SSPF incorporated a 65° arrow wing, twin vertical tails, and a canard. The SSPF was also equipped with unconventional controls including deflectable wingtips (tiperons) and pitch and yaw thrust vectoring in addition to conventional control surfaces. Before the free-flight tests, a direct eigenstructure assignment technique was used to design control laws that blended these unconventional and conventional control surfaces. The combined controls were intended to provide good flying characteristics well into the poststall angle-of-attack region.

In general, the SSPF exhibited good flying characteristics up to an angle of attack of 80°. Flights made with reduced feedback gains indicated significant robustness in the control law design. Use of thrust vectoring, blended with conventional pitch and yaw control surfaces, provided good stability and control characteristics throughout the angle-of-attack range tested. The tiperons, coupled with conventional ailerons, provided adequate roll control up to an angle of attack of 70°. Overall, free-flight tests indicated that it was possible to blend effectively conventional and unconventional control surfaces to achieve good flying characteristics well into the poststall angle-of-attack region.

Introduction

The desire for aircraft with sustained and efficient supersonic cruise performance has resulted in configurations with high-fineness-ratio fuselages, highly swept low-aspect-ratio wings, and highly integrated control surfaces. Configurations that incorporate these features, which are conducive to low cruise drag (ref. 1), generate strong vortical flows. These vortical flows and their breakdown can lead to nonlinear aerodynamic characteristics and high levels of instability. Powerful control devices that maintain their effectiveness at high angles of attack must be used to stabilize and control such configurations adequately. The challenge is to develop a flight control system that blends these control devices in order to maintain good flying characteristics well into the poststall angle-of-attack region. One method for evaluating both the stability and control characteristics of a configuration and the effectiveness of a flight control system is the use of the wind-tunnel free-flight test technique.

Wind-tunnel free-flight tests have been conducted at the Langley Research Center since the late 1930's (ref. 2). From its early beginnings to the present investigation, the free-flight test technique has focused on obtaining qualitative data about the dynamic stability and control characteristics of aircraft at moderate to high angles of attack. Free-flight testing of dynamically scaled models is an important test technique for understanding the complex aerodynamics and nonlinear flight mechanics associated with modern fighter aircraft at high angles of attack. Free-flight testing can also qualitatively evaluate potential flight control systems. With properly scaled mass and inertial characteristics, a scale model of an aircraft can be thought of as a simulator that has all the vehicle aerodynamics and interactions properly modeled.

The configuration used in the present investigation, called the supersonic persistence fighter or SSPF (ref. 1), is shown in figure 1. The SSPF configuration is the result of a series of previous wind-tunnel studies conducted as part of a cooperative program between the NASA Langley Research Center (LaRC) and the McDonnell Aircraft Company (MCAIR). The purpose of these studies was to develop a low-speed design data base for supersonic cruise configurations (refs. 1, 3, 4, and 5). Past investigations focused on the effect of component integration on airframe stability characteristics and the development of advanced control devices such as thrust vectoring and the use of deflectable wingtips. Results of previous investigations of the static and dynamic aerodynamic characteristics of the SSPF are presented in reference 6. The present report will focus on the results of a recent free-flight investigation of the SSPF. Limited results from reference 6 are presented to aid in the analysis and discussion of results from the recent free-flight tests. A discussion of the control law development process that preceded the free-flight tests is also presented.

Symbols

All data were initially measured in the body-axis system shown in figure 2. Longitudinal force and moment data are presented in the stability-axis system; lateral-directional force and moment data are presented in the body-axis system.

b	wingspan, ft
C_D	drag coefficient, $\frac{\text{Drag}}{\bar{q}S}$
C_L	lift coefficient, $\frac{\text{Lift}}{\bar{q}S}$
$C_{L,\max}$	maximum lift coefficient

C_l	rolling-moment coefficient, $\frac{\text{Rolling moment}}{\bar{q}Sb}$
C_m	pitching-moment coefficient, $\frac{\text{Pitching moment}}{\bar{q}S\bar{c}}$
C_n	yawing-moment coefficient, $\frac{\text{Yawing moment}}{\bar{q}Sb}$
C_Y	side-force coefficient, $\frac{\text{Side force}}{\bar{q}S}$
$\bar{c}$	mean aerodynamic chord, excluding trailing-edge extension, ft
f	frequency of oscillation, cycles/sec
g	acceleration due to gravity, 32.17 ft/sec^2
I_x, I_y, I_z	mass moments of inertia about X, Y, and Z body axes, slug-ft^2
k	reduced-frequency parameter, $\frac{\omega b}{2V}$
N_y	lateral acceleration, g units
p, q, r	angular velocity about X, Y, and Z body axes, rad/sec
$\bar{q}$	free-stream dynamic pressure, lb/ft
S	wing area, excluding trailing-edge extension, ft^2
s	frequency domain independent variable, 1/sec
u, v, w	linear velocity along X, Y, and Z body axes, ft/sec
V	free-stream velocity, ft/sec
X, Y, Z	body axes
α	angle of attack, deg
β	angle of sideslip, deg
$\dot{\beta}$	rate of change of sideslip, rad/sec
ΔC_l	incremental rolling-moment coefficient
ΔC_n	incremental yawing-moment coefficient
ΔC_Y	incremental side-force coefficient
δ_a	aileron deflection, positive for left roll, deg
δ_c	canard deflection, positive trailing-edge down, deg
δ_F	trailing-edge extension flap deflection, positive trailing-edge down, deg
δ_f	leading-edge flap deflection, positive leading-edge down, deg
δ_{pv}	pitch-vane deflection, positive trailing-edge down, deg
δ_r	rudder deflection, positive trailing-edge left, deg
δ_{wt}	wingtip deflection, positive for left roll, deg
δ_{yv}	yaw-vane deflection, positive trailing-edge left, deg
ζ_d	dutch roll damping ratio
ζ_{sp}	short period damping ratio
τ_R	roll-mode time constant, sec
ω	angular velocity, $2\pi f$, rad/sec
ω_d	dutch roll frequency, rad/sec
ω_{sp}	short period frequency, rad/sec

Stability derivatives:

$$C_{l_p} = \frac{\partial C_l}{\partial \frac{pb}{2V}} \quad C_{l_r} = \frac{\partial C_l}{\partial \frac{rb}{2V}} \quad C_{l_\beta} = \frac{\partial C_l}{\partial \beta} \quad C_{l_{\dot{\beta}}} = \frac{\partial C_l}{\partial \frac{\dot{\beta}b}{2V}}$$

$$C_{m_q} = \frac{\partial C_m}{\partial \frac{qc}{2V}} \quad C_{m_\alpha} = \frac{\partial C_m}{\partial \alpha}$$

$$C_{n_p} = \frac{\partial C_n}{\partial \frac{pb}{2V}} \quad C_{n_r} = \frac{\partial C_n}{\partial \frac{rb}{2V}} \quad C_{n_\beta} = \frac{\partial C_n}{\partial \beta} \quad C_{n_{\dot{\beta}}} = \frac{\partial C_n}{\partial \frac{\dot{\beta}b}{2V}}$$

$$C_{Y_p} = \frac{\partial C_Y}{\partial \frac{pb}{2V}} \quad C_{Y_r} = \frac{\partial C_Y}{\partial \frac{rb}{2V}} \quad C_{Y_\beta} = \frac{\partial C_Y}{\partial \beta} \quad C_{Y_{\dot{\beta}}} = \frac{\partial C_Y}{\partial \frac{\dot{\beta}b}{2V}}$$

$$C_{n_{\beta,\text{dyn}}} = C_{n_\beta} \cos\alpha - \frac{I_z}{I_x} C_{l_\beta} \sin\alpha$$

Abbreviations:

alpha	filtered angle of attack
BetaF	filtered angle of sideslip
BetDot	estimated rate of change of sideslip
BL	butt line
c.g.	center of gravity
DEA	direct eigenstructure assignment
FCL	flight control laws
LE	leading edge
MCAIR	McDonnell Aircraft Company
MS	model station
Pejector	ejector pressure
PIO	pilot-induced oscillations
Pstab	stability-axis roll rate
qbar	tunnel free-stream dynamic pressure

Rstab	stability-axis yaw rate
RTES	real-time-engineering simulation
SQR	square root
SSPF	supersonic persistence fighter
TEX	trailing-edge extension

Model

Tests were made with a 0.14-scale model of the SSPF in the Langley 30- by 60-Foot Tunnel. A sketch of the SSPF and details of the wing, canard, vertical tails, and control surfaces can be found in figure 3. Geometric, mass, and inertial characteristics of the SSPF free-flight model are presented in table I. The model had an arrow wing with a 65° swept leading edge and an aspect ratio of 1.95. A close-coupled canard was mounted just above the engine inlets. Deflectable surfaces on the wing included leading-edge flaps, ailerons, and tiperons (deflectable wingtips). In addition to the canard, a flap at the end of the trailing-edge extension (TEX) was used for pitch control (fig. 3(b)). Twin vertical tails, incorporating conventional rudders, were canted inboard 15° and mounted on the outboard edge of the trailing-edge extension. The model was also equipped with thrust vectoring in both pitch and yaw axes. Angular deflections of all moving surfaces were measured perpendicular to their respective hinge lines; the ranges of deflections are given in table II.

During free-flight testing, the model was equipped with two multiport ejectors (fig. 4(a)) supplied with compressed air to generate thrust. Secondary air from the model engine inlets was entrained with the high-pressure air from the ejector. The primary (high-pressure) air and the secondary (inlet) air were mixed as they flowed to the exhaust nozzles. A photograph of the thrust-vectoring vane arrangement is presented in figure 4(b). Geometric details of the vanes are given in table I. The ejectors and thrust-vectoring vanes, used only during free-flight tests, were calibrated at wind-off conditions. The model was unpowered, with flow through inlets, during conventional static and dynamic force and moment tests.

Test and Apparatus

Static and Dynamic Tests

Static and dynamic force tests were conducted in the Langley 30- by 60-Foot Tunnel at a free-stream dynamic pressure of 10 psf, which corresponded to a Reynolds number of 1.89×10^6, based on the wing mean aerodynamic chord. Aerodynamic force and moment data were measured with an internal six-component strain-gauge balance. Static data were obtained over an angle-of-attack range of 0° to 65° at angles of sideslip of 0° and ±5°. These data were obtained for a moment reference center of $0.36\bar{c}$, which corresponds to the one used for free-flight tests. Flow angularity corrections were made for both angle of attack and angle of sideslip. Basic aerodynamic data, including static stability derivatives and control effectiveness, were obtained during static force tests. Lateral-directional derivatives were calculated from data obtained at the $\beta = \pm 5°$ conditions.

A second investigation in the Langley 30- by 60-Foot Tunnel was conducted to determine the aerodynamic damping characteristics of the SSPF in the roll and yaw axes. A small-amplitude forced-oscillation technique combined balance force and moment outputs with the known angular position of the model to calculate aerodynamic damping characteristics (see ref. 7 for a complete description of the forced-oscillation test technique). These tests were conducted at a dynamic pressure of 10 psf with a moment reference center of $0.38\bar{c}$. Data were obtained over an angle-of-attack range of 0° to 90°. Forced-oscillation tests were conducted at an amplitude of ±5° and a frequency of 0.75 Hz. Use of this frequency resulted in a reduced-frequency parameter k of 0.13. All captive force and moment tests were conducted with flow-through inlets and the model unpowered.

Free-flight tests

Free-flight tests were conducted in the Langley 30- by 60-Foot Tunnel to assess stability and controllability of the SSPF and the effects of control law design on these characteristics. All flights were made with a moment reference center of $0.36\bar{c}$. During free-flight tests, the model was powered by compressed air (using the ejector system previously described) and was flown unrestrained in the open-throat test section of the tunnel (figs. 5(a) and (b)). The conditions represented $1g$, wings-level flight; angle of attack was varied by trimming the model at different dynamic pressures. Flights were conducted over an angle-of-attack range of 20° to 80°. The model was remotely controlled by three pilots: a roll and yaw pilot, a pitch pilot, and a thrust pilot. Air lines and signal wires were contained in an umbilical line that led from the top of the test section to the model. During flights the umbilical was kept slack by a safety cable operator to minimize its effect on the model motions. A sketch of the free-flight test setup is shown in figure 5(c).

The model was equipped with a three-axis rate gyro for measuring body-axis pitch, roll, and yaw

rates. A miniaturized α/β vane sensor was boom mounted from the model nose. A three-axis accelerometer was also installed in the model to measure body-axis accelerations. Only the lateral acceleration signal was intended for use during these tests. Output from these sensors was used to augment the stability characteristics of the SSPF through the use of a fly-by-wire control system. The primary component of this fly-by-wire control system was a digital computer programmed with the control laws. This system was designed to allow in-flight variations of key control law parameters such as gains, filter constants, and control surface command limits. The computer combined pilot command signals with data signals from the model sensors and computed the appropriate control surface commands. The control surfaces, moved using electropneumatic actuators, were capable of moving the model control surfaces at more than 120°/sec. All inputs to the computer and all commands to the model were updated at 10-msec intervals.

Control Law Development

The control laws for the SSPF free-flight model were generated using a direct eigenstructure assignment (DEA) synthesis technique for angles of attack up to 65°. Because aerodynamic data did not exist above an angle of attack of 65°, the control laws were linearly extrapolated for flights made beyond this angle of attack. This multivariable, model-following technique uses a set of desired eigenvalues and eigenvectors as its design goals. The desired eigenspace is chosen so that the dynamic system it describes will meet a given set of flying-qualities criteria. A weighted least-squares-solution algorithm is then used to obtain the control gains.

DEA is an output feedback formulation that does not offer the guaranteed stability margins of linear quadratic techniques; however, it is not constrained to full-state feedback so the control system designer can specify the variables used as feedbacks. The DEA technique also has the potential to include many higher order dynamics in the system model without a significant increase in complexity of the control system. Further discussion and examples of the methodology and use of DEA can be found in references 8 through 13.

The flying-qualities design goals for the SSPF were initially based on requirements specified in reference 14. However, these guidelines were developed at low angles of attack; recent studies (refs. 15 through 17) show that different design goals are required at higher angles of attack. A set of design goals (short period, dutch roll, and roll-mode characteristics) was determined with the guidelines of references 14 through 17. Although full-scale aircraft modes could be used as given, the desired dynamics could not be determined until the specified frequencies were increased to model scale. Guidelines for control system robustness of 6 dB gain margin and 45° phase margin were determined from reference 18. These robustness guidelines were strictly followed throughout the control system design process.

The model of desired dynamics for the SSPF, to be used in the control law synthesis, was developed primarily with the VECTOR program (ref. 19). VECTOR allows the designer to determine the aircraft control effector requirements and stability augmentation capability for a configuration from basic aircraft geometry and aerodynamic data (fig. 6(a)). Inputs to VECTOR include geometry, weight and inertias, aerodynamic characteristics (such as C_L and C_D), and control surface rate and deflection limits. A simple engine model that represented the ejectors used in the free-flight tests was used for the VECTOR inputs. After the data entries have been made, VECTOR allows the designer to vary these data inputs parametrically to study their effect on flying characteristics. VECTOR results for the SSPF were used to determine the desired eigenstructure models necessary for the DEA control law synthesis.

A MCAIR in-house program entitled SCHEDULE was also used extensively during the development of the SSPF free-flight control laws. Using SCHEDULE, the designer can quickly set up control surface schedules for trim and assess the effect that these schedules have on lift, drag, and stability and control characteristics (fig. 6(b)). SCHEDULE can also be used to evaluate the impact of trim deflections on aerodynamic control requirements and center-of-gravity (c.g.) movement.

A parametric study was conducted to determine the best c.g. location for the SSPF. The final choice of c.g. location ($0.36\bar{c}$) represented a trade-off between stability, control power, and trim requirements. SCHEDULE was then used to develop a canard schedule, based on angle of attack, to improve the basic nonlinear longitudinal stability characteristics of the airframe. Figure 7 illustrates the stability improvements obtained from the SCHEDULE analysis. The canard schedule eliminated a pitch-up problem and resulted in a uniform stability level at angles of attack less than 30°. SCHEDULE was also used to ensure that the final canard schedule did not adversely affect the lateral-directional stability characteristics of the SSPF.

With the given model of desired dynamics developed from the VECTOR results, the control law synthesis was performed using the DEA technique. The block diagrams for the resulting control laws, including additional switches used during free-flight tests for evaluation of the control system, are presented in figures 8(a) through (c). The longitudinal axis was an angle-of-attack command system. Proportional angle-of-attack and pitch-rate feedbacks were used to stabilize the airframe and provide the desired longitudinal flying qualities. The lateral axis used a roll-rate command system; the directional axis used a sideslip-angle command system. Cross feeds were included between the roll and yaw commands to ensure roll and yaw coordination without the use of pilot yaw command inputs. For the $1g$, wings-level flight conditions encountered during free-flight tests, these cross feeds allowed simultaneous lateral and directional axis control. Roll rate, yaw rate, angle of sideslip, and estimated time-rate-of-change of sideslip angle were used as feedbacks in the lateral-directional axes to augment stability and to improve flying qualities. The control law design blended all available control devices, including pitch and yaw thrust vectoring, as a function of angle of attack. The baseline gain schedules, determined from the control law synthesis and initial free-flight tests, and the final gain schedules are shown in figure 9. These two gain schedules are listed in appendixes A and B.

The SSPF control laws were evaluated with both linear and nonlinear methods. The linear evaluation methods included equivalent systems and stability margin analysis. The results of the linear analysis are shown in figure 10. Although the desired flying qualities were not achieved at every angle of attack, in general the desired characteristics were obtained. The stability margin analysis showed that gain margins above 15 dB and phase margins beyond 60° were achieved for the entire angle-of-attack range. A full nonlinear six-degree-of-freedom batch simulation was also conducted for the SSPF. A final step in the analysis of the SSPF free-flight control laws was a real-time piloted simulation with the MCAIR real-time-engineering simulation (RTES) package (fig. 11), which consists of a Silicon Graphics IRIS work station and a Digital Equipment VAX computer. The IRIS provided the pilot-vehicle interface and the required graphics; the six-degree-of-freedom equations were computed on the VAX. This simulation provided a pilot-in-the-loop validation of the control law design. Because the aircraft could be flown from any perspective, including outside the aircraft, the free-flight test environment could be simulated. All the evaluations indicated that the stability margins and control response of the SSPF met the desired flying-qualities and robustness guidelines. A detailed account of the SSPF control system design process can be found in reference 20.

Captive Test Summary

The purpose of the present investigation was to use the free-flight test technique to evaluate the SSPF flying characteristics and flight control system. A summary of the existing data base on the SSPF is presented to facilitate analysis of the free-flight results. Both static and dynamic force and moment data are presented with the leading-edge flap deflected ($\delta_f = 30°$) to correspond with the configuration used during free-flight tests. Additional data and further discussion of these results are found in reference 6.

Static Force Tests

Results from static force tests are presented in figures 12 through 15(a) and 15(b). The pitching-moment data of figure 12 show that the SSPF was slightly unstable for most canard deflections with a slight pitch-up near $\alpha = 25°$. Although this phenomenon is common for highly swept wings, the onset angle of attack was lower than expected because of the placement of the vertical tails (ref. 4). With the canard deflected $-40°$, the configuration was stable for low angles of attack and exhibited a severe pitch-up near $\alpha = 15°$. This change in the pitching-moment characteristics, common for large negative canard deflections (see refs. 21 and 22), is believed to result from the canard wake interacting with the wing flow field. For angles of attack of about 30° to 35°, a sharp, stable break was evident in pitching moment for all canard deflections.

The canard was scheduled with angle of attack to improve the longitudinal stability characteristics of the SSPF, and linear pitching-moment characteristics (fig. 8) were achieved up to an angle of attack of 30°. Beyond an angle of attack of 30°, canard effectiveness decreased rapidly, and other means of stability augmentation were required. The pitch control provided by the TEX flaps, shown in figure 13, was adequate for stability augmentation and trim up to $C_{L,\max}$. At poststall angles of attack, all trim capability and stability augmentation in the longitudinal axis were provided by thrust vectoring. The control effectiveness associated with thrust vectoring will be discussed later.

The static lateral-directional characteristics exhibited by the SSPF are presented in figure 14 and are generally representative of modern fighter aircraft (refs. 21 and 22). Lateral stability increased

sharply with increasing angle of attack for low angles, as expected for a highly swept wing configuration. The expected decrease in lateral stability near maximum lift, also common with highly swept wings, was reduced by the influence of the vertical tails (see ref. 4). The placement of the vertical tails caused symmetric bursting of the strong wing leading-edge vortices, thereby delaying the decrease in static lateral stability. Directional stability decreased with angle of attack, and the configuration became unstable at angles of attack above 20° to 25°. For $\alpha > 45°$, the forebody vortex system dominated the flow field and resulted in a stabilizing increment to C_{n_β} (ref. 2). At angles of attack between 15° and 30°, nonzero canard deflections decreased directional stability. In the poststall angle-of-attack region, only the larger canard deflections affected C_{n_β}. With the canard highly loaded ($\delta_c = 20°$) directional stability was decreased, whereas with the canard unloaded ($\delta_c = -40°$) directional stability was improved.

Lateral-directional control characteristics are shown in figures 15(a) and (b). The ailerons, though quite effective at low angles of attack, rapidly became ineffective past $\alpha = 20°$ as flow over the wing became parallel to the aileron hingeline (ref. 2). The tiperons, designed to take advantage of this spanwise flow, remained effective at higher angles of attack and produced little or no yawing moment. Combined, the ailerons and tiperons provided good body-axis roll control throughout the angle-of-attack range tested (fig. 15(a)). Figure 15(b) shows that the twin rudders were effective for providing yaw control up to an angle of attack of 40°. Beyond that point, rudder effectiveness rapidly decreases; therefore, thrust vectoring in yaw would be necessary for directional control.

Forced-Oscillation Tests

Results of the forced-oscillation tests are summarized in figures 16 and 17. Negative values for roll damping ($C_{l_p} + C_{l_\beta} \sin\alpha$) and yaw damping ($C_{n_r} - C_{n_\beta} \cos\alpha$) are stable. The SSPF exhibited stable, although low, roll damping characteristics throughout the angle-of-attack range tested. Canard deflection had minimal effect on roll damping. The only exception was $\delta_c = -40°$, where roll damping decreased to zero near $\alpha = 30°$. Canard deflection had a more pronounced effect on yaw damping, particularly at angles of attack near 15° and 40° (fig. 17). Near $\alpha = 15°$, yaw damping decreased as canard deflection was changed from −40° to 20°. The opposite effect, with a larger change in magnitude, was seen near $\alpha = 40°$. These results, when combined with those for static directional stability, indicate that the canard is interacting with the forebody flowfield characteristics. Above about an angle of attack of 50°, the SSPF exhibited unstable yaw damping; changes in canard deflection had no effect.

Forced-oscillation tests were not conducted in the pitch axis; however, pitch-damping characteristics were estimated with the strip theory method described in reference 23. The pitch-damping estimation shown in figure 18 indicates that the SSPF should exhibit stable pitch-damping characteristics throughout the angle-of-attack range of interest.

Thrust Calibration Tests

Static wind-off thrust tests were conducted to determine the effectiveness of the pitch and yaw thrust-vectoring vanes. The results from these tests are presented in figure 19 for two thrust levels. Changes in pitching moment with pitch-vane deflection were linear for deflections between ±10°. For deflections greater than +10° (nose down), the pitch vanes were slightly less effective; for deflections less than −10°, the pitch vanes were slightly more effective. This trend was independent of thrust level. Yawing moment exhibited linear behavior for yaw-vane deflections between ±20°, with a slight decrease in effectiveness for greater deflections. The turning efficiency for both the pitch and yaw vanes, defined as the ratio of thrust deflection to vane deflection, averaged about 55 percent. Variation was less than 3 percent as thrust levels and deflection angles varied.

Figure 20 illustrates the pitch and yaw control available with thrust vectoring. The crosshatched area represents the pitch and yaw control envelope as a function of angle of attack. These coefficients are based on dynamic pressures and thrust levels calculated from the aerodynamic data base for the SSPF for trimmed, 1g flight (see fig. 21). As angle of attack increases, thrust levels increase and dynamic pressure decreases; the result is increased pitch and yaw control effectiveness. Even at an angle of attack of 20°, thrust-vectoring control far exceeds the effectiveness of the conventional aerodynamic controls.

Free-Flight Test Results

To aid in the analysis of the free-flight results, the trim stability derivatives for the SSPF were calculated for wings-level, 1g flight conditions based on the aerodynamic data presented earlier. These calculations were made with the flight control laws (FCL) inactive and for the baseline and the minimum FCL gains determined during free-flight tests. The results from this analysis are presented in figures 21

through 25. The yaw divergence parameter $C_{n_{\beta,\mathrm{dyn}}}$ was calculated from these results and is also included. The results in figures 22 through 25 were based on the predicted values of dynamic pressure and thrust levels at trimmed flight conditions determined from the data base.

Baseline Longitudinal Characteristics

Initial free-flight investigations of the baseline flight characteristics of the SSPF were made at angles of attack between 21° and 50°. The baseline configuration consisted of the SSPF geometry shown in figure 3, with the leading-edge flaps deflected 30° and the gain schedules listed in appendix A. Initial flights indicated that the baseline control system for the SSPF provided sufficient stability augmentation for good flying characteristics in pitch throughout the angle-of-attack range tested. Good flying characteristics can be defined as follows: (1) good response, (2) quick damping of disturbances, and (3) low pilot work load. Pitch control, which was blended between the TEX flaps and pitch vanes depending on angle-of-attack, was good at all angles of attack tested without any noticeable loss in control power at the higher angles of attack. Reduced pitch-vane gains compensated for the higher thrust levels associated with high-α flight conditions. This gain reduction successfully prevented potential overcontrol of the model in pitch.

Longitudinal Gain Variations

The longitudinal characteristics of the SSPF were further evaluated by reducing the level of angle-of-attack and pitch-rate feedback to the TEX flaps and pitch vanes. At angles of attack below 30°, good flying characteristics could be maintained even when the α feedback was reduced by 50 percent. The model could be flown, however, at angles of attack below 30° without α feedback, even though the configuration was statically unstable (fig. 22(a)). The high levels of augmented pitch damping (fig. 22(b)) were sufficient to maintain control without α feedback. Pilot workload, however, was significantly increased without α feedback, and the model was highly susceptible to pilot-induced oscillations (PIO) which resulted in unacceptable flying characteristics in pitch. Above an angle of attack of 30° the SSPF was statically stable in pitch, and flights made at higher angles of attack indicated that α feedback, as expected, was not necessary for good flying characteristics.

Variations of pitch-rate feedback indicated that this gain could be reduced 50 percent and still maintain good pitch-damping characteristics throughout the angle-of-attack range tested. Although the configuration could not be flown without pitch-rate feedback, flights below an angle of attack of 30° were possible with pitch-rate feedback reduced by 75 percent. With this reduced gain, however, the pitch-damping characteristics of the SSPF were marginal. Pitch oscillations were slow to damp out, and constant pilot attention was necessary to avoid a pitch departure. Flights were also made with both angle-of-attack and pitch-rate feedbacks reduced. These flights indicated that angle-of-attack and pitch-rate feedback gains could both be reduced to 50 percent of nominal values and still maintain good flying characteristics with light pilot workload.

Baseline Lateral-Directional Characteristics

Initial free-flight evaluations of the lateral-directional characteristics of the SSPF were made at angles of attack between 21° and 50°. During these initial flights the model accelerometer malfunctioned and resulted in a lateral acceleration signal that was unreliable. Because of this malfunction, the washed-out yaw rate and lateral acceleration portions of the $\dot{\beta}$ estimator were eliminated from the control laws by setting $Yk10 = 0$ (see fig. 8(e)). This modified $\dot{\beta}$ estimator was used for all flights discussed in this report.

The original β feedback gain provided highly stable values of C_{n_β} at all angles of attack. This high-gain β feedback system, combined with the high gain on the modified $\dot{\beta}$ feedback, caused some problems during initial checkout flights. Therefore, the gains on these two feedbacks were reduced to 10 percent of the original values. All references to the baseline control system include this reduction in the β and $\dot{\beta}$ feedback gains. These initial flights also indicated that, for angles of attack below 25°, β and $\dot{\beta}$ feedbacks to the yaw control surfaces overstabilized the configuration. It is believed that the loss of the lateral acceleration component in the $\dot{\beta}$ estimator was partially responsible for this behavior. As angle of attack increased above 25°, β and $\dot{\beta}$ feedback did not adversely affect flying characteristics. However, these feedbacks did not appear necessary at high angles of attack, even though the configuration became directionally unstable (fig. 23(a)). A possible explanation for this result is indicated by the directional divergence parameter $C_{n_{\beta,\mathrm{dyn}}}$ shown in figure 24. Positive values of this parameter indicate that a configuration has a tendency to resist a yaw divergence (refs. 4 and 24). The stable values of C_{l_β} exhibited by the SSPF (fig. 23(b)) are sufficient to maintain positive values of $C_{n_{\beta,\mathrm{dyn}}}$ at all angles

of attack tested. Because of this tendency to resist a yaw divergence, the SSPF appears more stable directionally than the static data of figure 23(a) indicate. Because β and $\dot{\beta}$ feedback to the yaw control surfaces did not enhance the static and dynamic directional stability characteristics of the SSPF, all remaining flights were made without these feedback paths.

Control characteristics of the SSPF were good throughout the angle-of-attack range tested. Good coordination between the roll and yaw axes was maintained by the cross feeds discussed previously. The aileron and tiperon surfaces provided good body-axis roll control at all angles of attack (see static data in fig. 15(a)). The yaw thrust vectoring, as expected, provided ample yawing moment for both directional control and directional stability augmentation. Damping characteristics in roll and yaw were also good at all angles of attack, as expected given the levels of augmented stability (figs. 25(a) and (b)). However, above an angle of attack of 40°, the configuration was slightly overdamped in roll, as indicated by the data of figure 25(b).

Lateral-Directional Gain Variations

Lateral-directional gain variations included: (1) β and $\dot{\beta}$ feedback reduction to the ailerons and tiperons, (2) roll- and yaw-rate feedback to the ailerons and tiperons, and (3) roll- and yaw-rate feedback to the rudders and yaw vanes. As the angle of attack was increased from 20° to 34°, β and $\dot{\beta}$ feedback to the ailerons and tiperons could gradually be reduced to zero without affecting the flying characteristics of the model. For all angles of attack beyond 34°, these two feedback paths could be eliminated.

A blend of roll- and yaw-rate feedback to the ailerons and tiperons augmented the roll-damping characteristics of the SSPF. Although $\dot{\beta}$ feedback also provided some enhancement to the roll-damping characteristics, the blended rate signal was the primary feedback used. Flights were possible throughout the angle-of-attack range without roll- and yaw-rate feedback to the ailerons and tiperons. Flights below an angle of attack of 42° indicated that modifications to the airframe roll-damping characteristics were necessary for smooth, controlled flights. Therefore, the blended roll- and yaw-rate feedback was increased to the baseline values as the angle of attack decreased from 42° to 21°.

To augment yaw damping, roll and yaw rates were blended for feedback to the rudders and yaw vanes. Flights were made throughout most of the angle-of-attack range with roll- and yaw-rate feedback to the rudders and yaw vanes reduced by 50 percent. At angles of attack below 30° and above 50°, the model was flyable with a 50-percent reduction in yaw-damping augmentation, although values closer to the baseline gains provided better flying characteristics and lower pilot workload. Flights made with reduced lateral-directional feedbacks indicated that the minimum gain levels determined with isolated gain reduction studies could be combined and still result in a stable, easily flown configuration.

Final Gain Schedules

Two flights were made at angles of attack between 21° and 80° using all the modified gain schedules determined in the gain variation studies. These modified gains are shown in figure 9 and listed in appendix B. Results from these flights indicated no unfavorable interactions between the longitudinal and lateral-directional axes as a result of combining the individual gain reductions. The SSPF, using the modified gain schedules, exhibited good stability characteristics throughout most of the angle-of-attack range tested, with adequate control authority to maneuver the model. Above an angle of attack of 70°, a significant loss in body-axis roll control required the pilot to rely on yaw control to maneuver the model in the lateral-directional axes. Finally, pitch damping above an angle of attack of 75° was also degraded, and the model exhibited small longitudinal oscillations similar to those typically seen when damping is low.

Concluding Remarks

Wind-tunnel free-flight tests have been conducted to examine the high-angle-of-attack stability and control characteristics and control law design of a supersonic persistence fighter (SSPF) at $1g$ flight conditions. In general, the SSPF exhibited good flying characteristics at angles of attack between 20° and 80°. A loss of roll control above an angle of attack of 70° and degraded pitch damping above an angle of attack of 75° were the only significant problem areas noted in the flight envelope. Flights made with reduced feedback gains indicated significant robustness in the control law design, which was a primary goal of the control law synthesis process. Cross feeds of pilot inputs between the lateral and directional axes provided good roll coordination at all angles of attack tested. Use of thrust vectoring blended with conventional pitch and yaw control surfaces provided good stability and control characteristics well into the poststall angle-of-attack region. Deflectable wingtips (tiperons) coupled with conventional ailerons provided adequate roll control up to an angle of attack of 70°.

Free-flight tests indicated that conventional and unconventional control surfaces could be blended to provide good flying characteristics well into the poststall angle-of-attack region for a configuration with highly nonlinear aerodynamic characteristics. These results show that the direct eigenstructure assignment technique for control law synthesis can yield very good designs. However, caution must be used in applying this technique as stability margins are not guaranteed.

NASA Langley Research Center
Hampton, VA 23681-0001
October 19, 1992

Appendix A

Baseline Control Law Gain Schedules

```
alpha2  =  alpha*alpha
Ptrim  =  -.01095*alpha2  +  2.808*alpha

SWITCHES  (all  nominally  closed)

        Longitudinal:  Sw1p,Sw2p,Sw3p,Sw4p,Sw5p,Sw6p
        Lateral:  Sw4r,Sw7r,Sw8r,Sw9r
        Directional:  Sw1r,Sw2r,Sw3r,Sw5r,Sw6r

LONGITUDINAL GAINS

Pk1  deg/unit  stick
        Pk1  =  -.372*alpha+24.84
        IF Pk1 <= 4 THEN Pk1 = 4

Pk2  deg/deg
        IF alpha < 24 THEN
            Pk2 = -.68
        ELSEIF alpha >= 30 THEN
            Pk2 = 0
        ELSE
            Pk2  =  -2.66  +  .0825*alpha
        END IF

Pk3   deg/(deg/sec)
        IF alpha < 24 THEN
            Pk3  =  -.0704*alpha  +  .363
        ELSE
            Pk3  =  -3.6577  +  .12535*alpha  -  .001175*alpha2
        END IF

Pk4   deg/(deg/sec)^2
        IF alpha < 30 THEN
            Pk4  =  -.017/(.128*alpha  -  5.76)
        ELSE
            Pk4  =  -.017/(-.547*alpha  +  14.52)
        END IF
        IF Pk4 < .0015 THEN Pk4 = .0015

Pk5,  Pk6  deg/deg
        Pk5  =  -.0833*alpha+3.5
        Pk6 = 1 - Pk5
        IF Pk5 < 0 THEN Pk5 = 0
        IF Pk5 > 1 THEN Pk5 = 1
        IF Pk6 < 0 THEN Pk6 = 0
        IF Pk6 > 1 THEN Pk6 = 1
        Pk6  =  Pk6*Ptrim/Pejector
```

```
Pk7  deg/deg
       Pk7  =  .044*alpha-1.85
       IF Pk7 > -.046 THEN Pk7 = -.046
       Pk7  =  Pk7*Ptrim/Pejector

Pk8  deg
       Pk8  =  .0833*alpha-3.165
       IF Pk8 < 0 THEN Pk8 = 0
       IF Pk8 > 1 THEN Pk8 = 1

LATERAL GAINS

Rk1  deg/unit  stick
       Rk1 = -.25*alpha + .5

Rk2  deg/unit  stick
       Rk2 = -.29 + .117*alpha - .00605*alpha2

Rk34  deg/deg
       Rk34 = 1

Rk3  deg/(deg/sec)
       Rk3 = -.022 + .00533*alpha - .000347*alpha2 +.0000072*alpha2*alpha
       IF Rk3 > .152 THEN Rk3 = .152
       Rk3 = Rk3*Rk34

Rk4  deg/(deg/sec)
       IF alpha < 36 THEN
          Rk4 = .0112*alpha - .187
       ELSEIF alpha >42 THEN
          Rk4 = .1
       ELSE
          Rk4 = -.0162*alpha + .8
       END IF
       IF Rk4 < .015 THEN Rk4 = .015
       Rk4 = Rk4*Rk34

Rk56  deg/deg
       Rk56 = 1

Rk5  deg/(deg/sec)
       IF alpha < 24 THEN
          Rk5 = .0165*alpha - .216
       ELSE
          Rk5 = 1.06 - .0584*alpha + .000919*alpha2
       END IF
       Rk5 = Rk5*Rk56
```

```
Rk6  deg/deg
      IF alpha < 12 THEN
         Rk6 = -1.3
      ELSEIF alpha > 42 THEN
         Rk6 = .0218*alpha - 1.946
      ELSE
         Rk6 = .5184 - .178*alpha + .00336*alpha2
      END IF
      Rk6 = Rk6*Rk56
```

DIRECTIONAL GAINS

```
Yk1  deg/unit  stick
      Yk1 = -96.1 + 3.25*alpha - .03*alpha2
      IF Yk1 < -50 THEN Yk1 = -50

Yk2  deg/unit  stick
      Yk2 = 18

Yk34  deg/deg
      Yk34 = 1

Yk3  deg/(deg/sec)
      IF alpha <= 42 THEN
         Yk3 = -.0229 - .0088*alpha + .000072*alpha2
      ELSEIF alpha >= 50 THEN
         Yk3 = -.186
      ELSE
         Yk3 = .0099*alpha - .68
      END IF
      Yk3 = Yk3*Yk34

Yk4  deg/(deg/sec)
      Yk4 = 1.1*(-.8499 + .0213*alpha - .00013*alpha2)
      IF Yk4 < -.45 THEN Yk4 = -.45
      IF Yk4 > -.065 THEN Yk4 = -.065
      Yk4 = Yk4*Yk34

Yk5  deg/(deg/sec)
      Yk5 = 4.9 - .1741*alpha + .00166*alpha2
      IF Yk5 > 2.3 THEN Yk5 = 2.3
      Yk5 = .1*Yk5

Yk6  deg/deg
      Yk6 = 13.73 - .439*alpha + .00376*alpha2
      IF Yk6 > 7.5 THEN Yk6 = 7.5
      Yk6 = .1*Yk6
```

```
Yk7  deg/deg
       Yk7 = -.0667*alpha + 2.667
       IF Yk7 > 1 THEN Yk7 = 1
       IF Yk7 < 0 THEN Yk7 = 0

Yk8  deg/deg
       Yk8 = .0375*alpha - .5
       IF Yk8 > 1 THEN Yk8 = 1
       IF Yk8 < .25 THEN Yk8 = .25
       Yk8 = Yk8*Ptrim/Pejector

Yk10  deg/g
       Yk10 = 1844/(29*SQR(qbar))
```

Appendix B

Modified Control Law Gain Schedules

```
alpha2  =  alpha*alpha
Ptrim  =  -.01095*alpha2  +  2.808*alpha

SWITCHES  (all  nominally  closed)

        Longitudinal:  Sw1p,Sw2p,Sw3p,Sw4p,Sw5p,Sw6p
        Lateral:  Sw4r,Sw7r,Sw8r,Sw9r
        Directional:  Sw1r,Sw2r,Sw3r,Sw5r,Sw6r

LONGITUDINAL GAINS

Pk1  deg/unit  stick
        Pk1  =  -.372*alpha+24.84
        IF Pk1 <= 4 THEN Pk1 = 4

Pk2  deg/deg
        IF alpha < 24 THEN
            Pk2 = -.34
        ELSEIF alpha >= 30 THEN
            Pk2 = 0
        ELSE
            Pk2  =  -1.7  +  .0567*alpha
        END IF

Pk3   deg/(deg/sec)
        IF alpha < 24 THEN
            Pk3  =  -.0704*alpha  +  .363
        ELSE
            Pk3  =  -3.6577  +  .12535*alpha  -  .001175*alpha2
        END IF
        Pk3  =  .5*Pk3

Pk4   deg/(deg/sec)2
        IF alpha < 30 THEN
            Pk4  =  -.017/(.128*alpha  -  5.76)
        ELSE
            Pk4  =  -.017/(-.547*alpha  +  14.52)
        END IF
        IF Pk4 < .0015 THEN Pk4 = .0015

Pk5,  Pk6  deg/deg
        Pk5  =  -.0833*alpha+3.5
        Pk6 = 1 - Pk5
        IF Pk5 < 0 THEN Pk5 = 0
        IF Pk5 > 1 THEN Pk5 = 1
        IF Pk6 < 0 THEN Pk6 = 0
        IF Pk6 > 1 THEN Pk6 = 1
        Pk6  =  Pk6*Ptrim/Pejector
```

```
Pk7  deg/deg
       Pk7  =  .044*alpha-1.85
       IF Pk7 > -.046 THEN Pk7 = -.046
       Pk7  =  Pk7*Ptrim/Pejector

Pk8  deg
       Pk8  =  .0833*alpha-3.165
       IF Pk8 < 0 THEN Pk8 = 0
       IF Pk8 > 1 THEN Pk8 = 1

LATERAL GAINS

Rk1  deg/unit  stick
       Rk1 = -.25*alpha + .5

Rk2  deg/unit  stick
       Rk2 = -.29 + .117*alpha - .00605*alpha2

Rk34  deg/deg
       IF alpha < 21 THEN
          Rk34 = 1
       ELSEIF alpha >= 43 THEN
          Rk34 = 0
       ELSE
          Rk34 = -.0455*alpha + 1.9545
       END IF

Rk3  deg/(deg/sec)
       Rk3 = -.022 + .00533*alpha - .000347*alpha2 +.0000072*alpha2*alpha
       IF Rk3 > .152 THEN Rk3 = .152
       Rk3 = Rk3*Rk34

Rk4  deg/(deg/sec)
       IF alpha < 36 THEN
          Rk4 = .0112*alpha - .187
       ELSEIF alpha >42 THEN
          Rk4 = .1
       ELSE
          Rk4 = -.0162*alpha + .8
       END IF
       IF Rk4 < .015 THEN Rk4 = .015
       Rk4 = Rk4*Rk34

Rk56  deg/deg
       IF alpha < 21 THEN
          Rk56 = 1
       ELSEIF alpha >= 34 THEN
          Rk56 = 0
       ELSE
          Rk56 = -.0769*alpha + 2.6154
       END IF
```

```
Rk5  deg/(deg/sec)
      IF alpha < 24 THEN
         Rk5 = .0165*alpha - .216
      ELSE
         Rk5 = 1.06 - .0584*alpha + .000919*alpha2
      END IF
      Rk5 = Rk5*Rk56

Rk6  deg/deg
      IF alpha < 12 THEN
         Rk6 = -1.3
      ELSEIF alpha > 42 THEN
         Rk6 = .0218*alpha - 1.946
      ELSE
         Rk6 = .5184 - .178*alpha + .00336*alpha2
      END IF
      Rk6 = Rk6*Rk56

DIRECTIONAL GAINS

Yk1  deg/unit  stick
      Yk1 = -96.1 + 3.25*alpha - .03*alpha2
      IF Yk1 < -50 THEN Yk1 = -50

Yk2  deg/unit  stick
      Yk2 = 18

Yk34  deg/deg
      IF alpha < 25 OR alpha > 60 THEN Yk34 = 1
      IF alpha > 30 AND alpha < 50 THEN Yk34 = .5
      IF alpha >= 25 AND alpha <= 30 THEN Yk34 = 1 - .1*(alpha - 25)
      IF alpha >= 50 AND alpha <= 60 THEN Yk34 = .5 + .05*(alpha - 50)

Yk3  deg/(deg/sec)
      IF alpha <= 42 THEN
         Yk3 = -.0229 - .0088*alpha + .000072*alpha2
      ELSEIF alpha >= 50 THEN
         Yk3 = -.186
      ELSE
         Yk3 = .0099*alpha - .68
      END IF
      Yk3 = Yk3*Yk34

Yk4  deg/(deg/sec)
      Yk4 = 1.1*(-.8499 + .0213*alpha - .00013*alpha2)
      IF Yk4 < -.45 THEN Yk4 = -.45
      IF Yk4 > -.065 THEN Yk4 = -.065
      Yk4 = Yk4*Yk34

Yk5  deg/(deg/sec)
      Yk5 = 0
```

```
Yk6  deg/deg
       Yk6 = 0

Yk7  deg/deg
       Yk7 = -.0667*alpha + 2.667
       IF Yk7 > 1 THEN Yk7 = 1
       IF Yk7 < 0 THEN Yk7 = 0

Yk8  deg/deg
       Yk8 = .0375*alpha - .5
       IF Yk8 > 1 THEN Yk8 = 1
       IF Yk8 < .25 THEN Yk8 = .25

Yk10  deg/g
       Yk10 = 1844/(29*SQR(qbar))
```

References

1. Klein, John R.; Walck, Kenneth J.; and Hahne, David E.: Airframe Component Effects on the Aerodynamic Stability and Control Characteristics of a Supersonic Cruise Fighter Aircraft at High Angles of Attack. AIAA-84-2110, Aug. 1984.

2. Campbell, John P.: *Free and Semi-Free Model Flight-Testing Techniques Used in Low-Speed Studies of Dynamic Stability and Control.* NASA TM X-50785, 1963.

3. Wood, Richard M.; Miller, David S.; Hahne, David E.; Niedling, Larry G.; and Klein, John R.: Status Review of a Supersonically-Biased Fighter Wing-Design Study. AIAA-83-1857, July 1983.

4. Hahne, David E.: *Low-Speed Aerodynamic Stability and Control Characteristics of an Advanced Fighter Aircraft at High Angles of Attack.* NASA TP-2617, 1986.

5. Marks, Bret A.; and Hahne, David E.: Innovative Control Concepts and Component Integration for a Generic Supercruise Fighter. *Aerodynamics of Combat Aircraft Controls and of Ground Effects*, AGARD-CP-465, Apr. 1990, pp. 10-1–10-14.

6. Hahne, David E.: *Low-Speed Static and Dynamic Force Tests of a Generic Supersonic Cruise Fighter Configuration.* NASA TM-4138, 1989.

7. Chambers, Joseph R.; and Grafton, Sue B.: *Static and Dynamic Longitudinal Stability Derivatives of a Powered 1/9-Scale Model of a Tilt-Wing V/STOL Transport.* NASA TN D-3591, 1966.

8. Schmidt, David K.; and Davidson, John B.: Flight Control Law Synthesis for an Elastic Vehicle by Eigenspace Assignment. AIAA-85-1898, Aug. 1985.

9. Wendel, Thomas R.: Flight Control Synthesis To Meet Flying Qualities Specifications: An Evaluation of Multivariable Synthesis Techniques. AIAA-87-2880, Sept. 1987.

10. Moore, B. C.: On the Flexibility Offered by State Feedback in Multivariable Systems Beyond Closed Loop Eigenvalue Assignment. *IEEE Trans. Autom. Control*, vol. AC-21, no. 5, Oct. 1976, pp. 689–692.

11. Cunningham, Thomas B.: Eigenspace Selection Procedures for Closed Loop Response Shaping With Modal Control. *Proceedings of the 19th IEEE Conference on Decision & Control Including the Symposium on Adaptive Processes*, Volume 1, IEEE Catalog No. 80CH1563-6, IEEE Control Systems Soc., 1980, pp. 178–186.

12. Andry, A. N., Jr.; Shapiro, E. Y.; and Chung, J. C.: Eigenstructure Assignment for Linear Systems. *IEEE Trans. Aerosp. & Electron. Syst.*, vol. AES-19, no. 5, Sept. 1983, pp. 711–729.

13. Sobel, Kenneth M.; and Shapiro, Eliezer Y.: Application of Eigenstructure Assignment to Flight Control Design: Some Extensions. *J. Guid., Control, & Dyn.*, vol. 10, no. 1, Jan. Feb. 1987, pp. 73–81.

14. Military Standard—*Flying Qualities of Piloted Aircraft.* MIL-STD-1797A, Jan. 30, 1990. (Supersedes MIL-STD-1797(USAF), Mar. 31, 1987.)

15. Krekeler, Gregory C., Jr.; Wilson, David J.; and Riley, David R.: High Angle of Attack Flying Qualities Criteria. AIAA-90-0219, Jan. 1990.

16. Wilson, David J.; and Riley, David R.: Flying Qualities for Stall/Post-Stall Angles of Attack. *High-Angle-of-Attack Technology*, Volume I, Joseph R. Chambers, William P. Gilbert, and Luat T. Nguyen, eds., NASA CP-3149, Part 2, 1992, pp. 569–585.

17. Wilson, David J.; and Riley, David R.: *Flying Qualities Criteria Development Through Manned Simulation for 45° Angle of Attack.* NASA CR-4311, July 1990.

18. *Military Specification—Flight Control System—General Specification For.* MIL-F-87242(USAF), U.S. Air Force, Mar. 31, 1986.

19. Smereczniak, P.: *Exhaust Nozzles for Aerocontrol. Volume I—Summary of Nozzle Static Test and Thrust Vectoring Utilization Results.* WRDC-TR-89-3068, Vol. I, U.S. Air Force, July 14, 1989. (Available from DTIC as AD B137 805.)

20. Wendel, Thomas R.; Boland, Joseph R.; and Hahne, David E.: High Angle of Attack Control Law Development for a Free-Flight Wind Tunnel Model Using Direct Eigenstructure Assignment. A Collection of Technical Papers, Volume 1—AIAA Guidance, Navigation and Control Conference, Aug. 1991, pp. 255–266. (Available as AIAA-91-2627-CP.)

21. Murri, Daniel G.; Nguyen, Luat T.; and Grafton, Sue B.: *Wind-Tunnel Free-Flight Investigation of a Model of a Forward-Swept-Wing Fighter Configuration.*

22. Murri, Daniel G.; Grafton, Sue B.; and Hoffler, Keith D.: *Wind-Tunnel Investigation and Free-Flight Evaluation of a Model of the F-15 STOL and Maneuver Technology Demonstrator.* NASA TP-3003, August 1990.

23. Thomas, R. W.: *Analysis of Aircraft Stability and Control Design Methods, Volume I.* AFWAL-TR-84-3038, Vol. I, U.S. Air Force, May 1984.

24. Moul, Martin T.; and Paulson, John W.: *Dynamic Lateral Behavior of High-Performance Aircraft.* NACA RM L58E16, 1958.

Table I. Mass, Inertial, and Geometric Characteristics of Model

Overall fuselage length, ft	9.38
Weight, lb	109.3
I_x, slugs-ft^2	1.51
I_y, slugs-ft^2	19.57
I_z, slugs-ft^2	20.26
Wing:	
Airfoil section	NACA 64A004
Span, ft	5.14
Area, ft^2	13.56
Mean aerodynamic chord, ft	3.22
Aspect ratio	1.95
Leading-edge sweep, deg	65
Aileron area (one side), ft^2	0.30
Tiperon area (one side), ft^2	0.29
Vertical tails:	
Airfoil section (root)	NACA 65A005
Airfoil section (tip)	NACA 65A003
Area (each), ft^2	1.56
Span, ft	1.29
Root chord, ft	1.96
Tip chord, ft	0.45
Aspect ratio	1.07
Leading-edge sweep, deg	62.8
Rudder area (each), ft^2	0.29
Trailing-edge extension:	
Length, ft	1.6
Width, ft	0.65
Flap area (each), ft^2	0.45
Canard:	
Airfoil section (root)	Biconvex ($t/c = 0.05$)
Airfoil section (tip)	Biconvex ($t/c = 0.03$)
Area, ft^2	1.36
Span, ft	1.84
Tip chord, ft	0.30
Aspect ratio	2.48
Leading-edge sweep, deg	50
Thrust-vectoring vanes:	
Pitch-vane area (each), ft^2	0.21
Pitch-vane chord, ft	0.25
Yaw-vane area (each), ft^2	0.05
Yaw-vane chord, ft	0.25

Table II. Deflection Range of Moving Surfaces

Surface	Deflection range, deg
LE flaps	0 to 30
Ailerons	±15
Tiperons	±30
TEX flaps	±30
Rudders	±30
Canard	−40 to 20
Pitch vanes	±25
Yaw vanes	±25

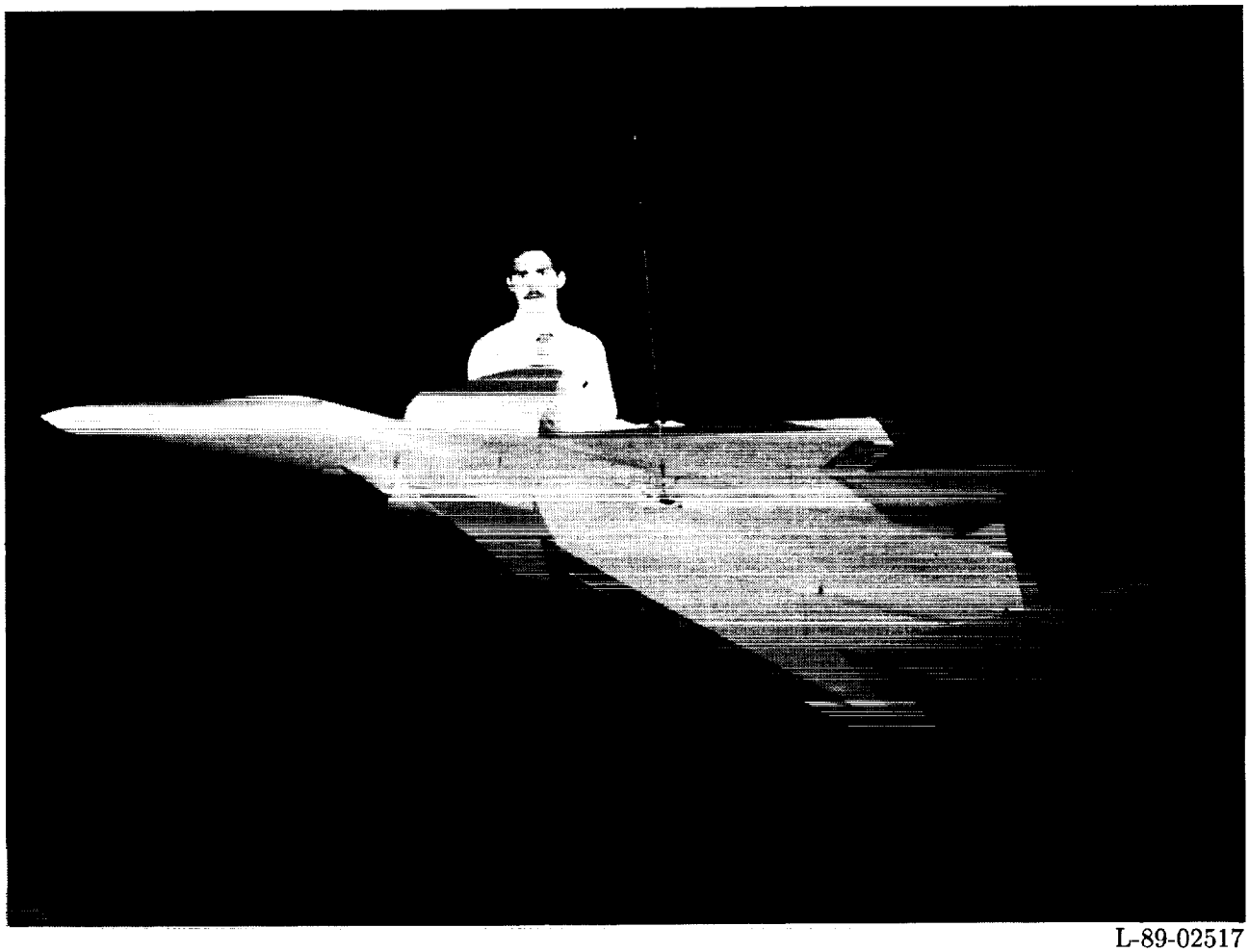

L-89-02517

Figure 1. Supersonic persistence fighter free-flight model.

ORIGINAL PAGE
BLACK AND WHITE PHOTOGRAPH

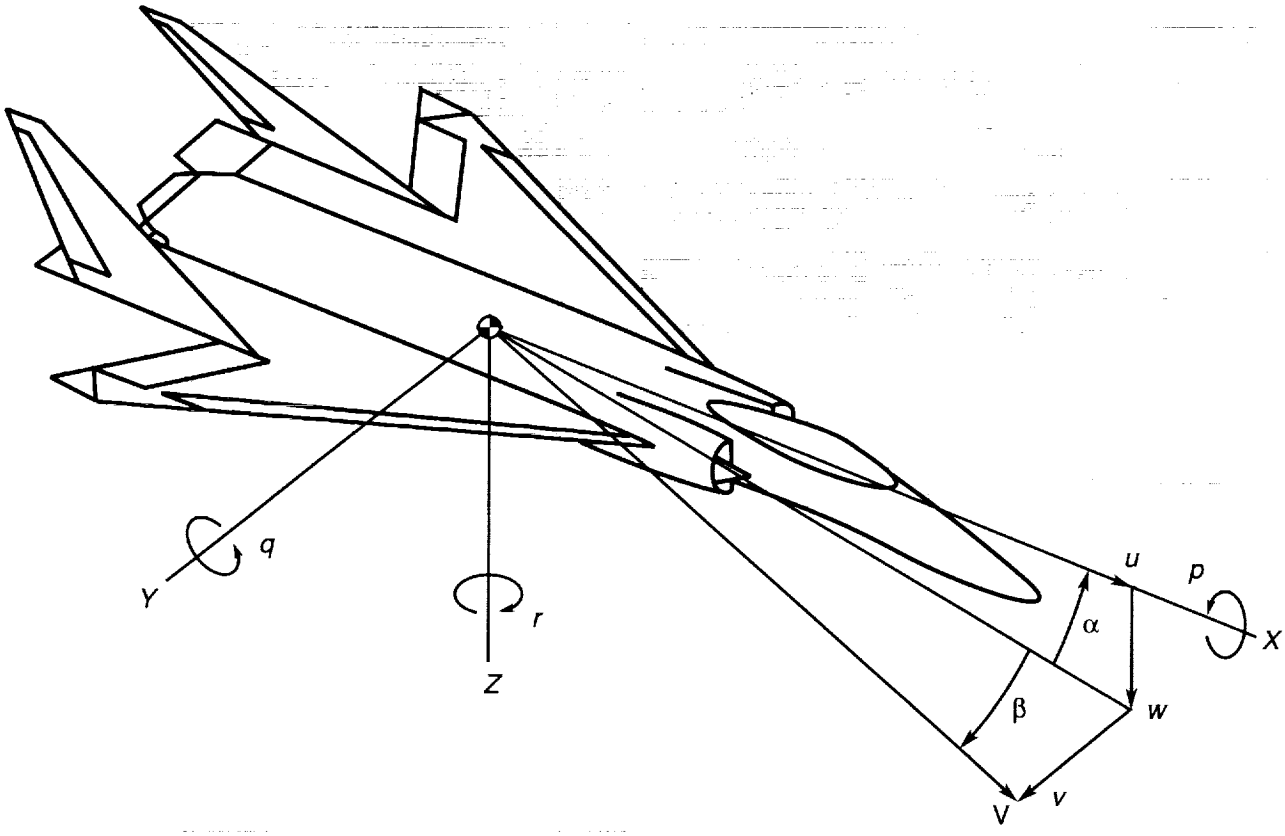

Figure 2. Definition of body-axis system.

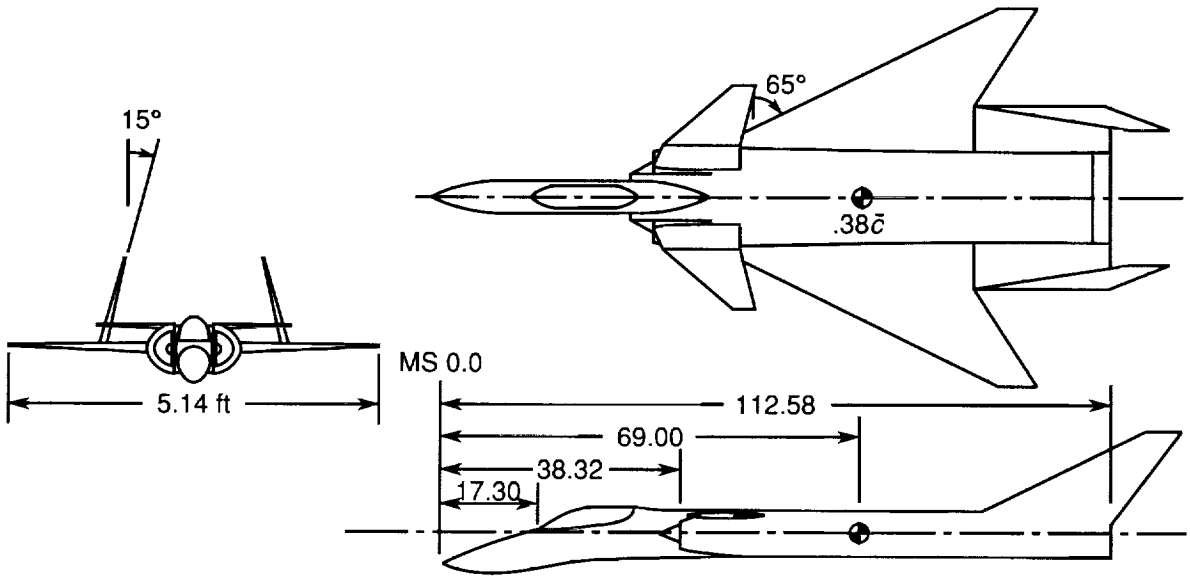

(a) Three-view sketch of model.

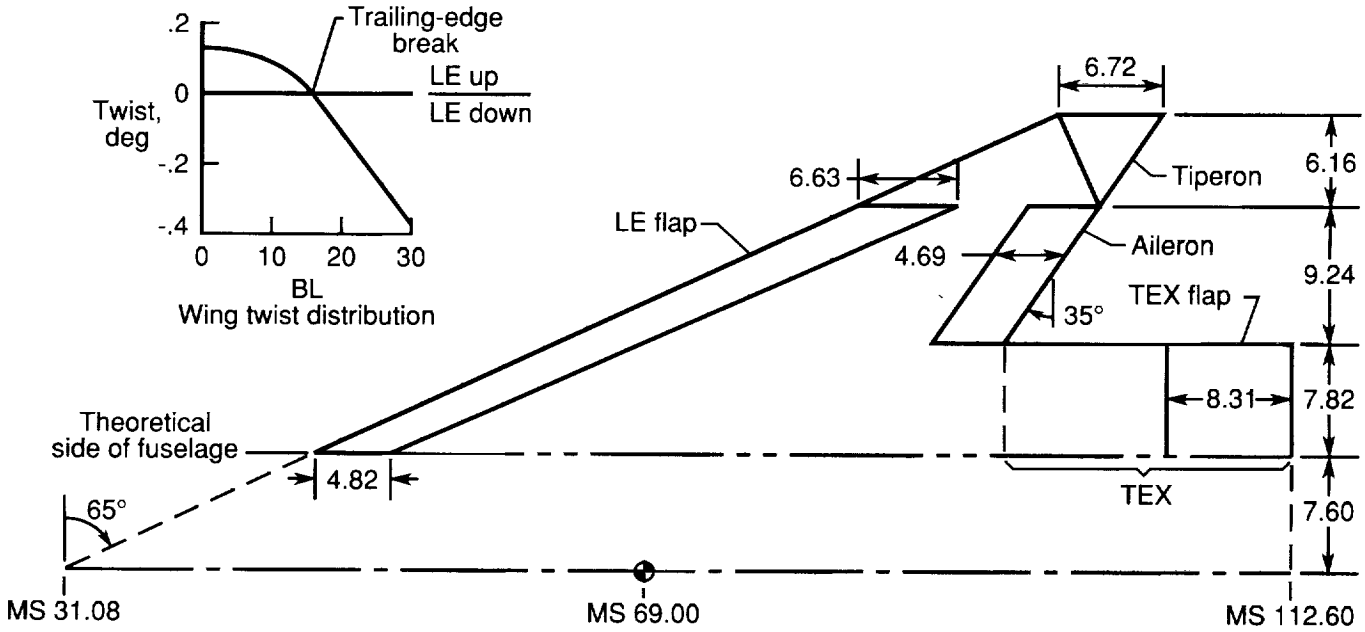

(b) Wing and TEX geometry; NACA 64A004 airfoil.

Figure 3. Details of baseline model geometry. Linear dimensions in inches except as noted.

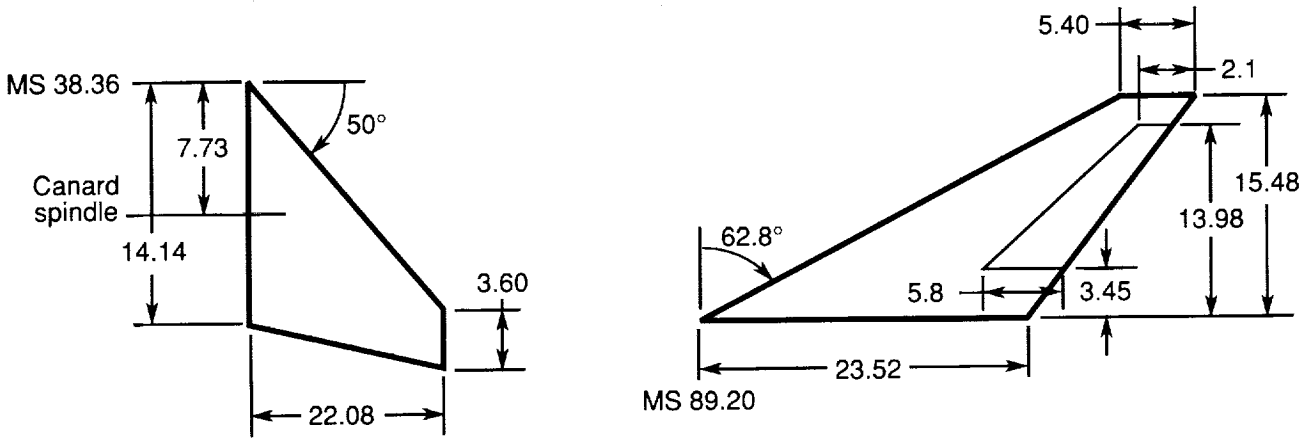

(c) Canard and vertical tail geometry.

Figure 3. Concluded.

L-90-31

(a) Ejector unit used to generate thrust.

Figure 4. Ejector and thrust-vectoring vanes.

ORIGINAL PAGE
BLACK AND WHITE PHOTOGRAPH

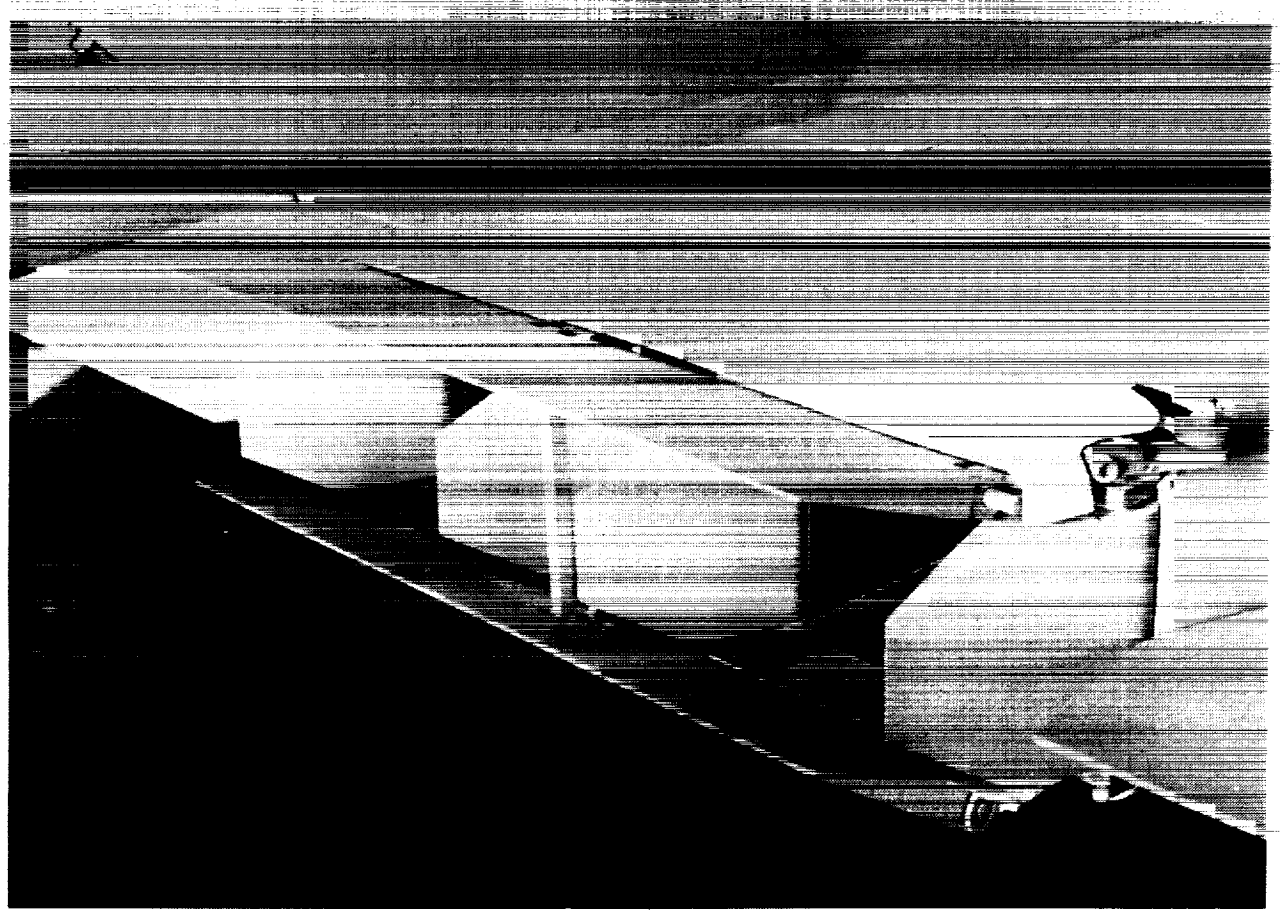

L-86-10,624

(b) Thrust-vectoring vanes.

Figure 4. Concluded.

ORIGINAL PAGE
BLACK AND WHITE PHOTOGRAPH

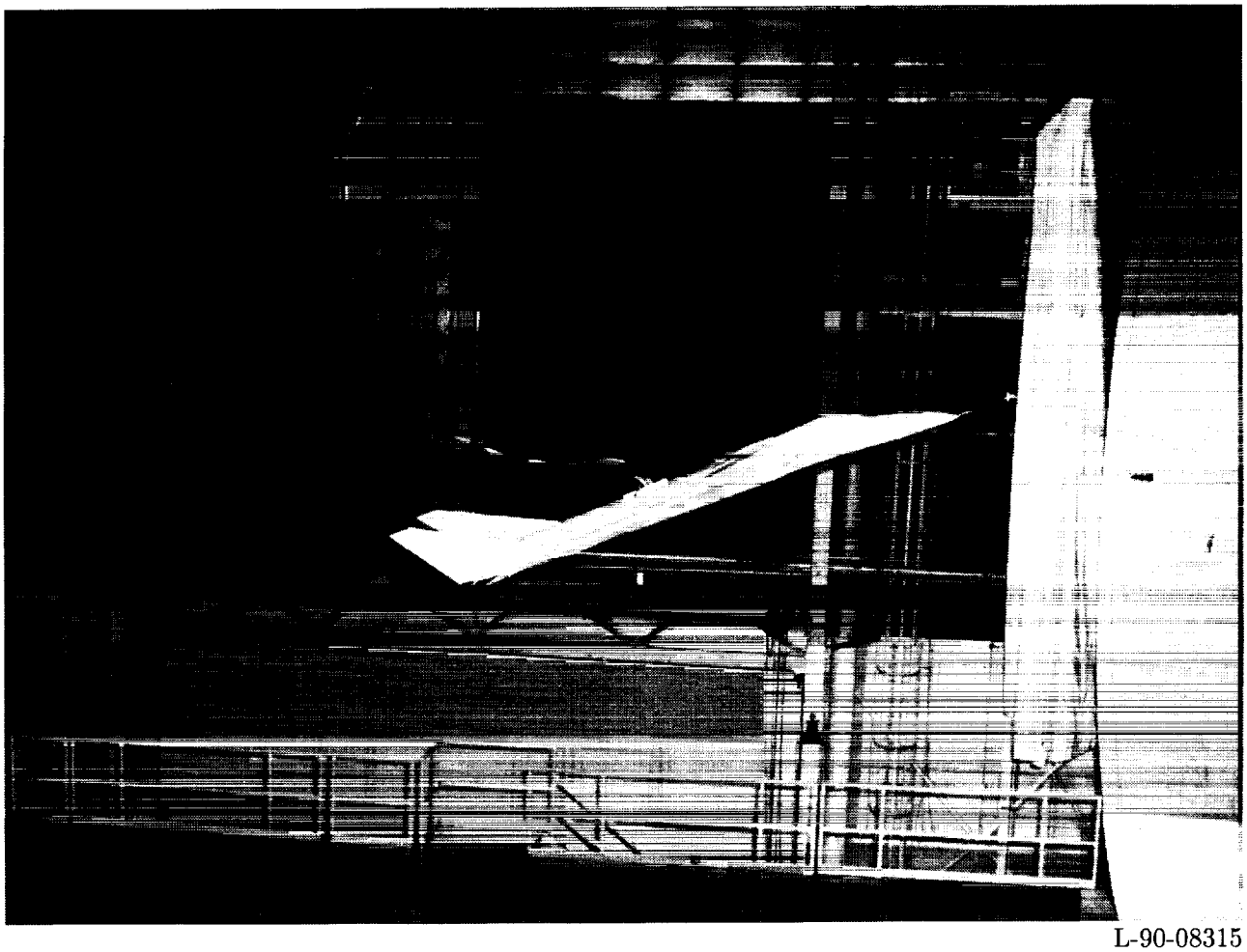

L-90-08315

(a) Side view of model in flight.

Figure 5. Free-flight test technique.

ORIGINAL PAGE
BLACK AND WHITE PHOTOGRAPH

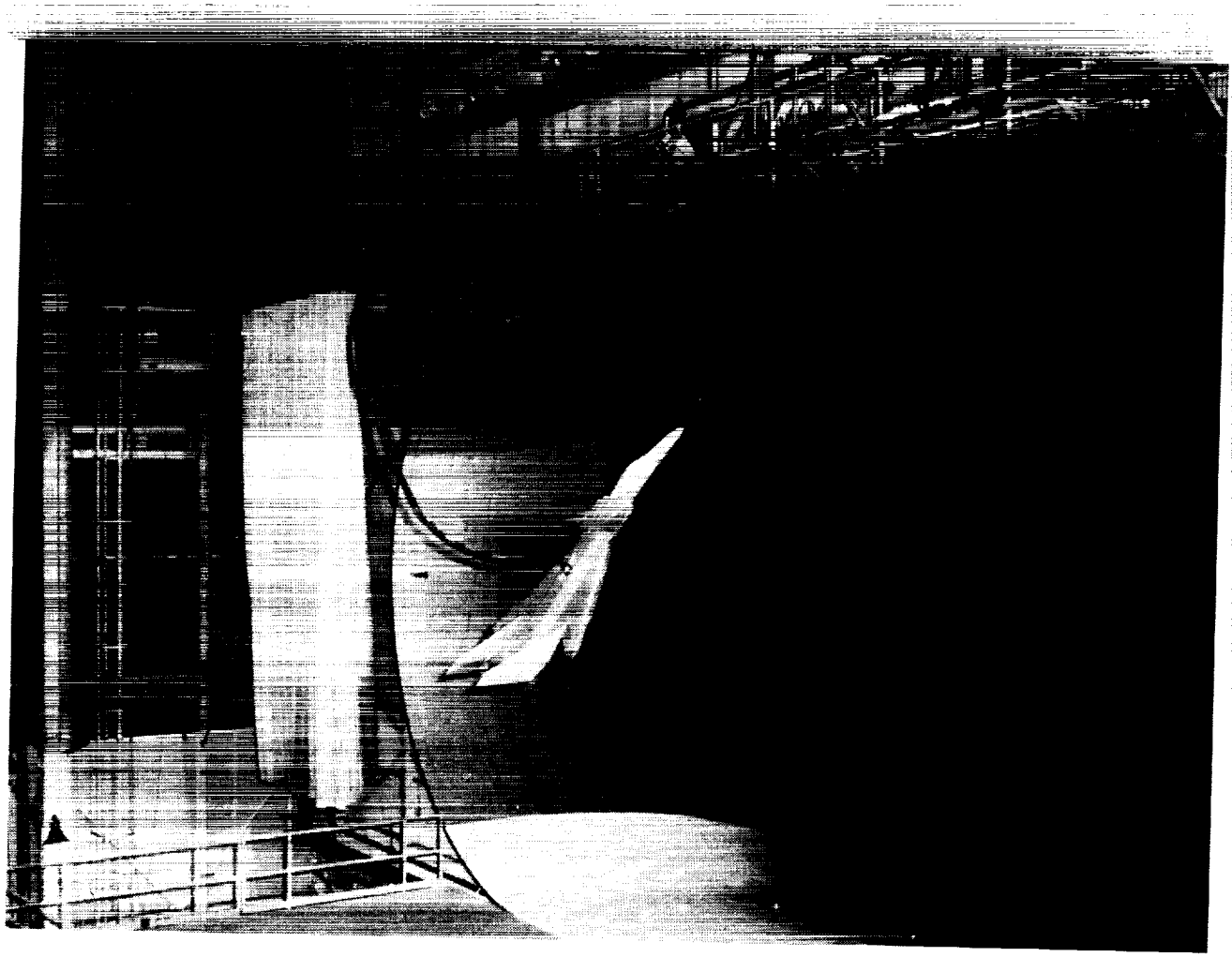

L-90-08311

(b) Three-quarter rear view of model in flight.

Figure 5. Continued.

ORIGINAL PAGE
BLACK AND WHITE PHOTOGRAPH

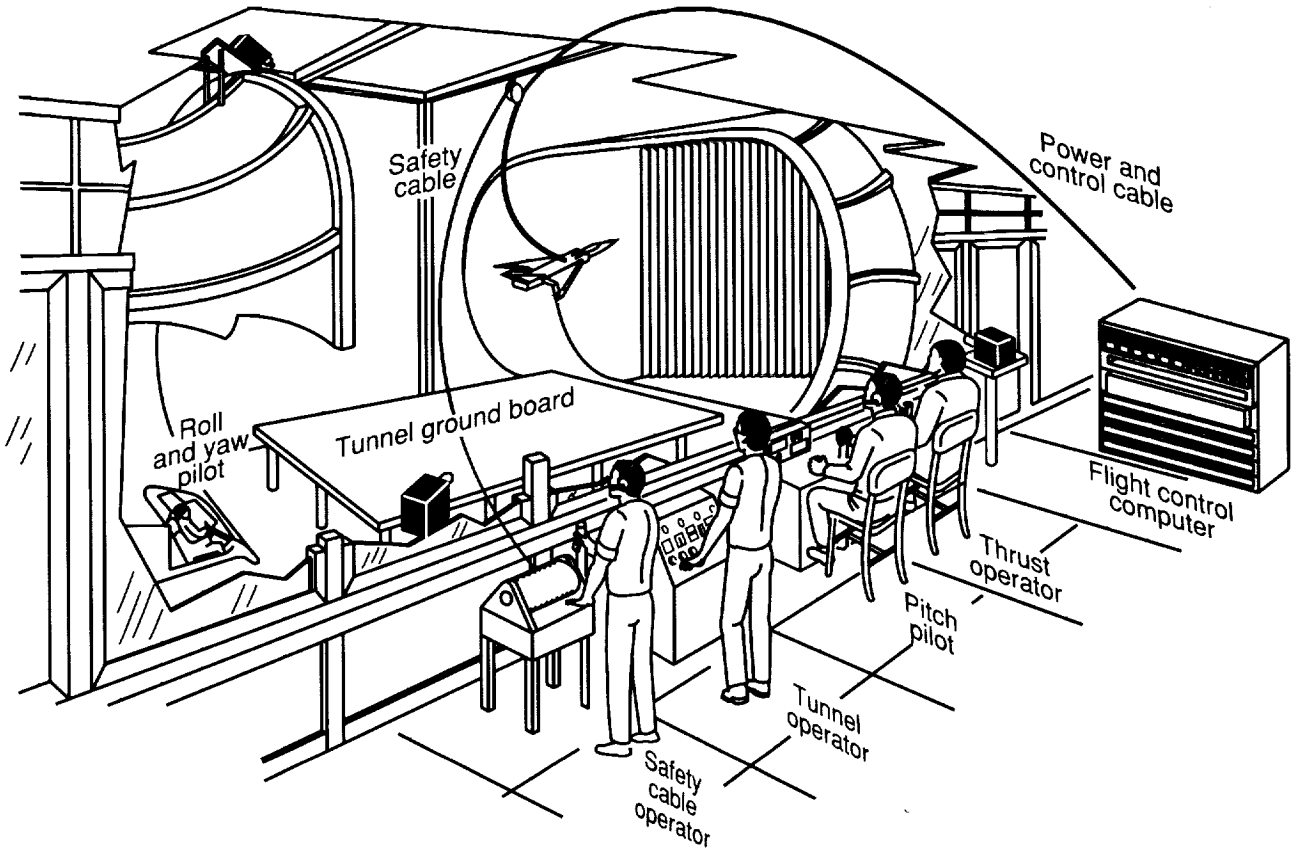

(c) Free-flight test setup.

Figure 5. Concluded.

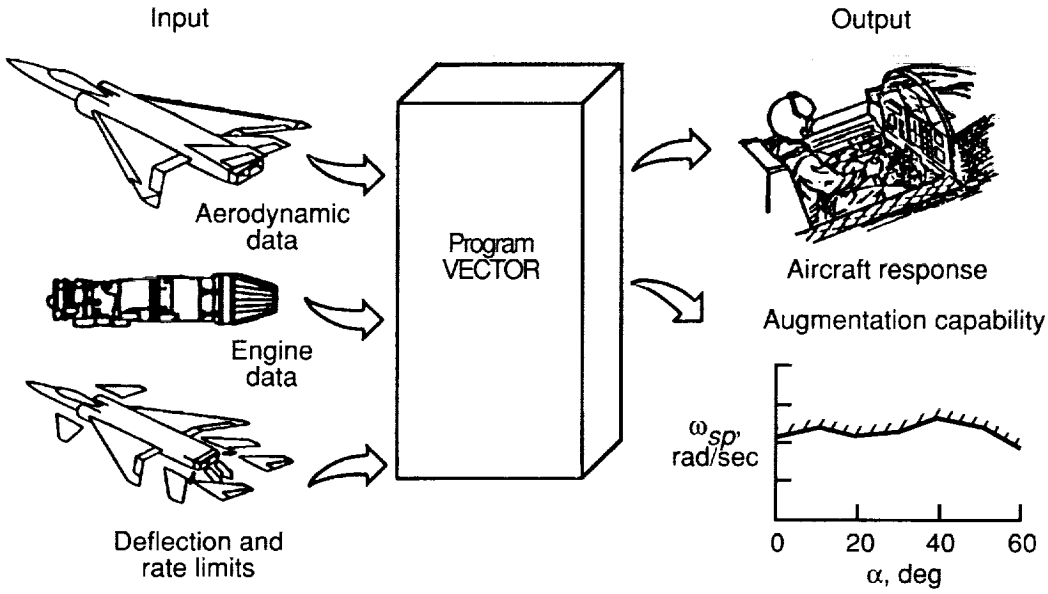

(a) Inputs and outputs of program VECTOR.

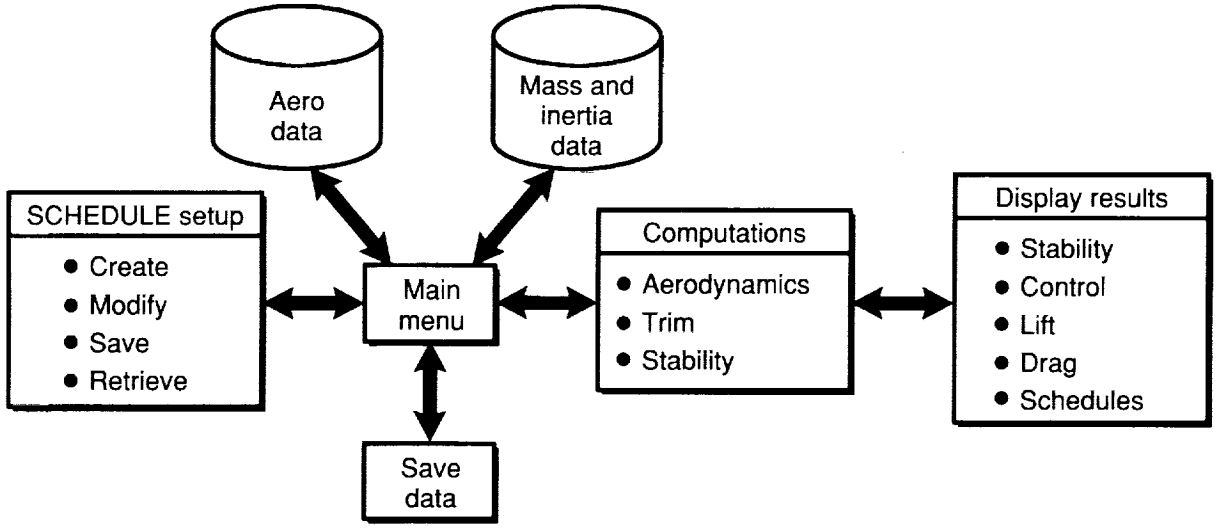

(b) Flow chart of program SCHEDULE.

Figure 6. Computer programs used in development of SSPF free-flight control laws.

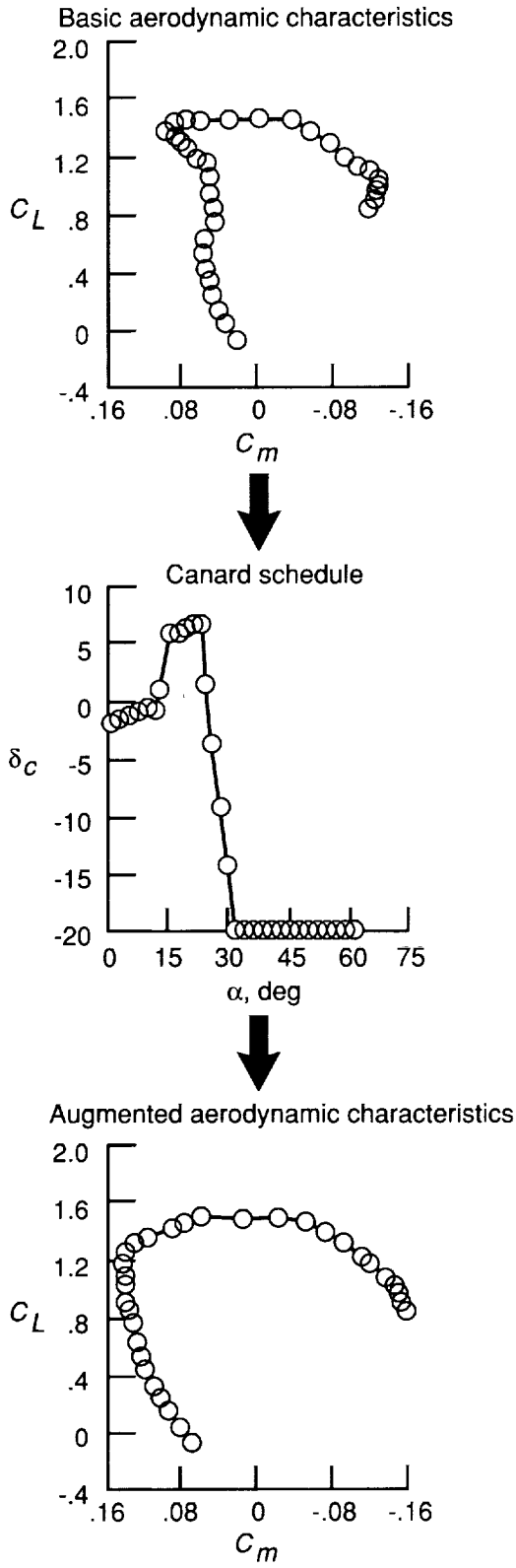

Figure 7. Effect of canard schedule on longitudinal stability.

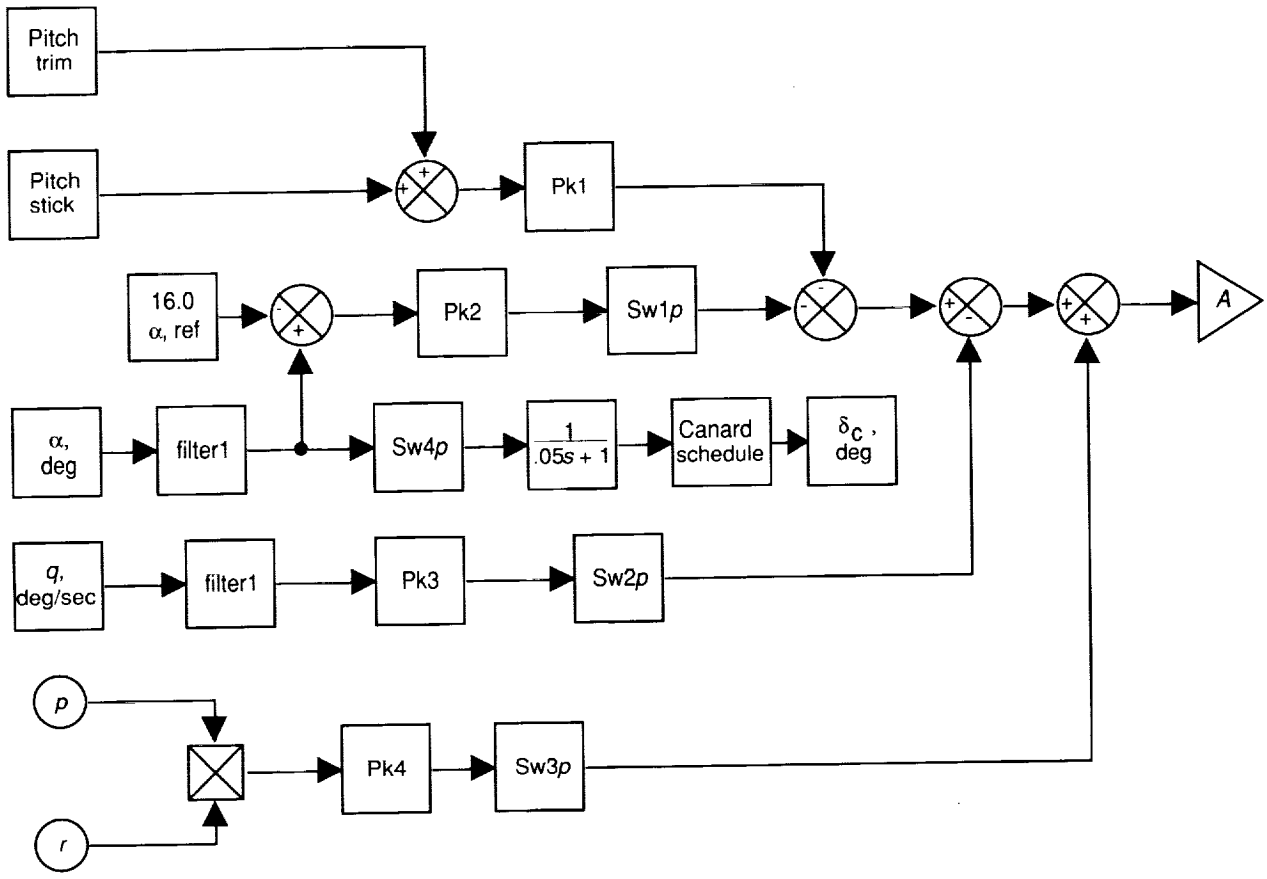

(a) Longitudinal feedback.

Figure 8. Block diagrams for free-flight model flight control system.

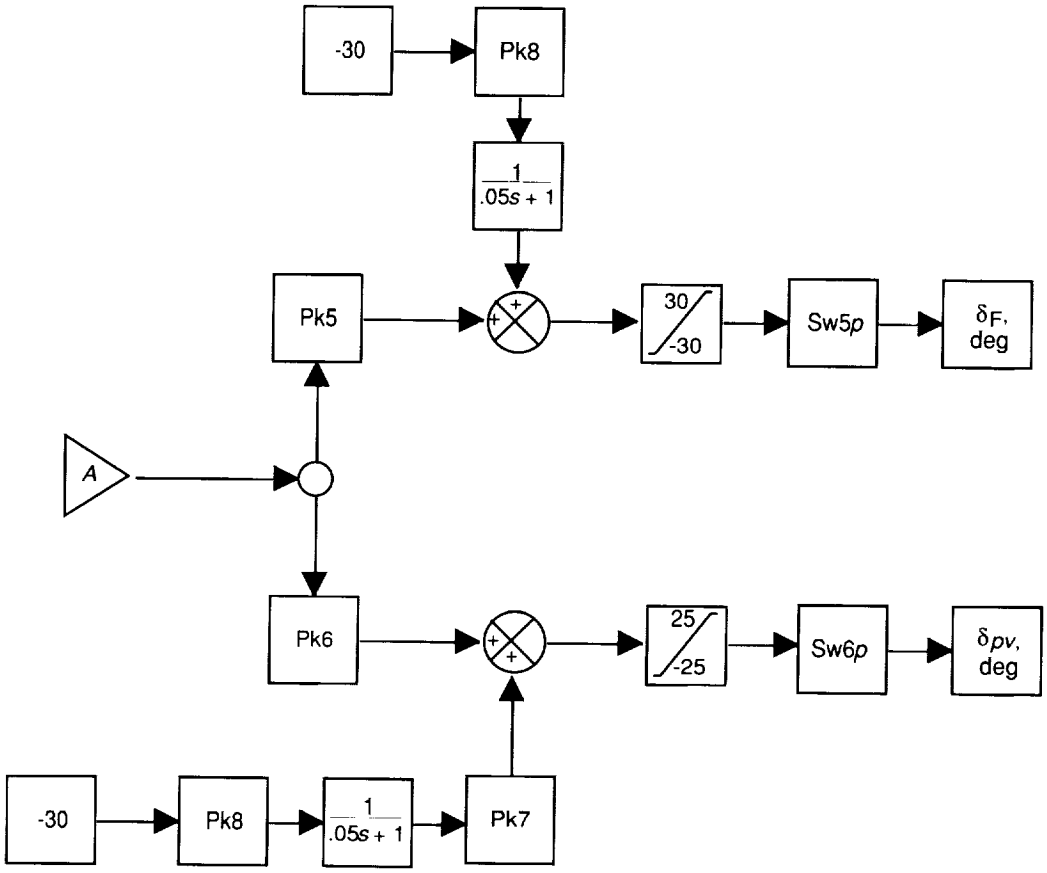

(b) Longitudinal control blending.

Figure 8. Continued.

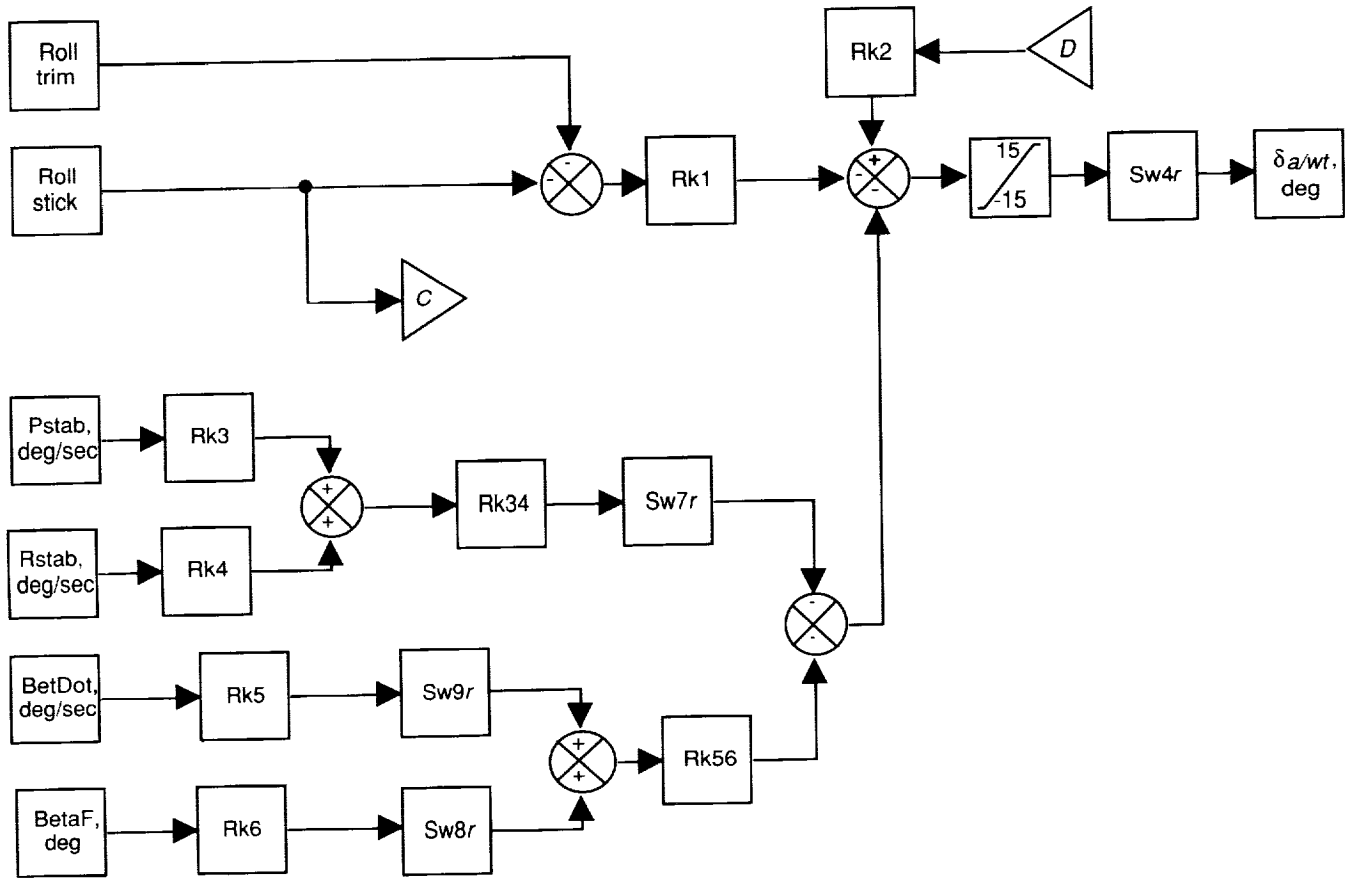

(c) Lateral feedback and control.

Figure 8. Continued.

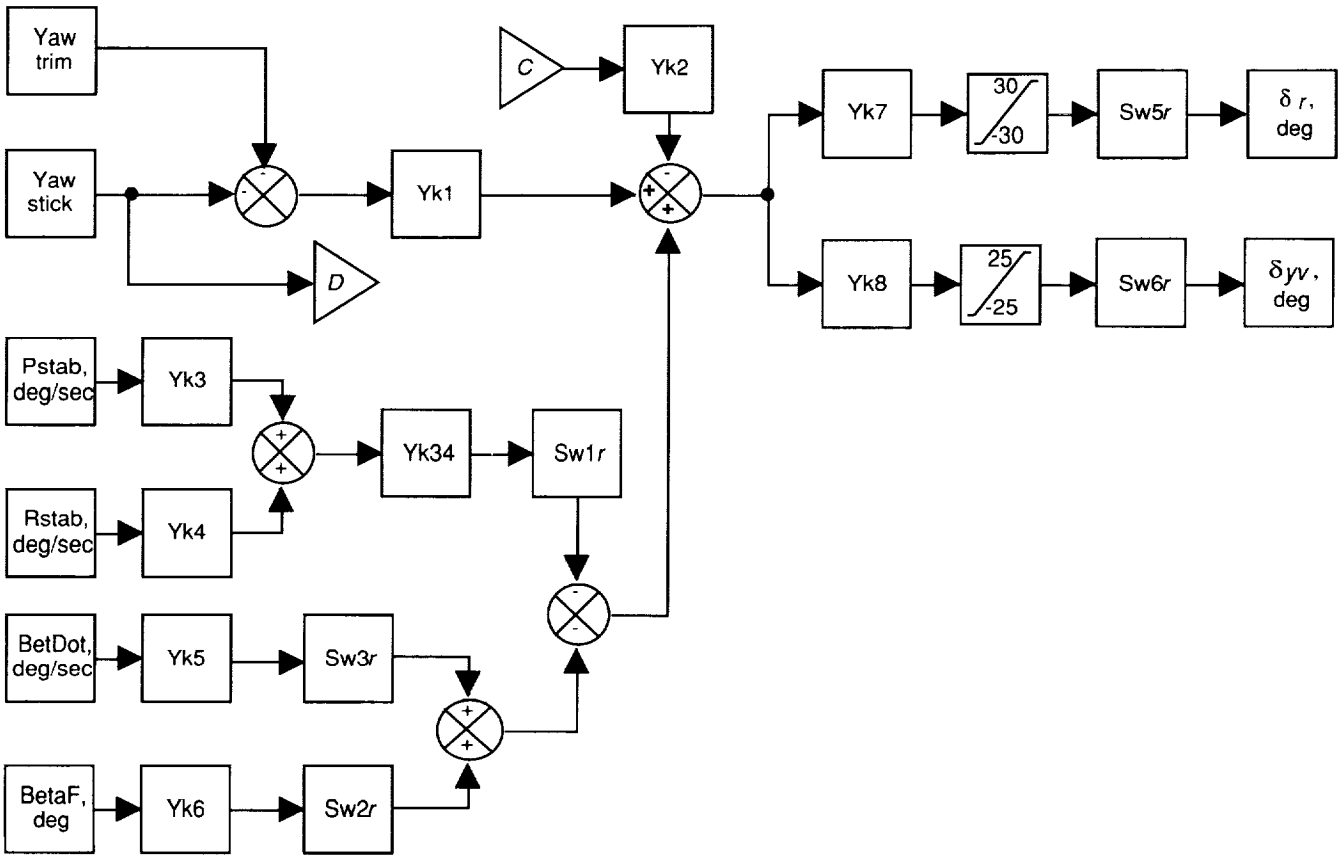

(d) Directional feedback and control.

Figure 8. Continued.

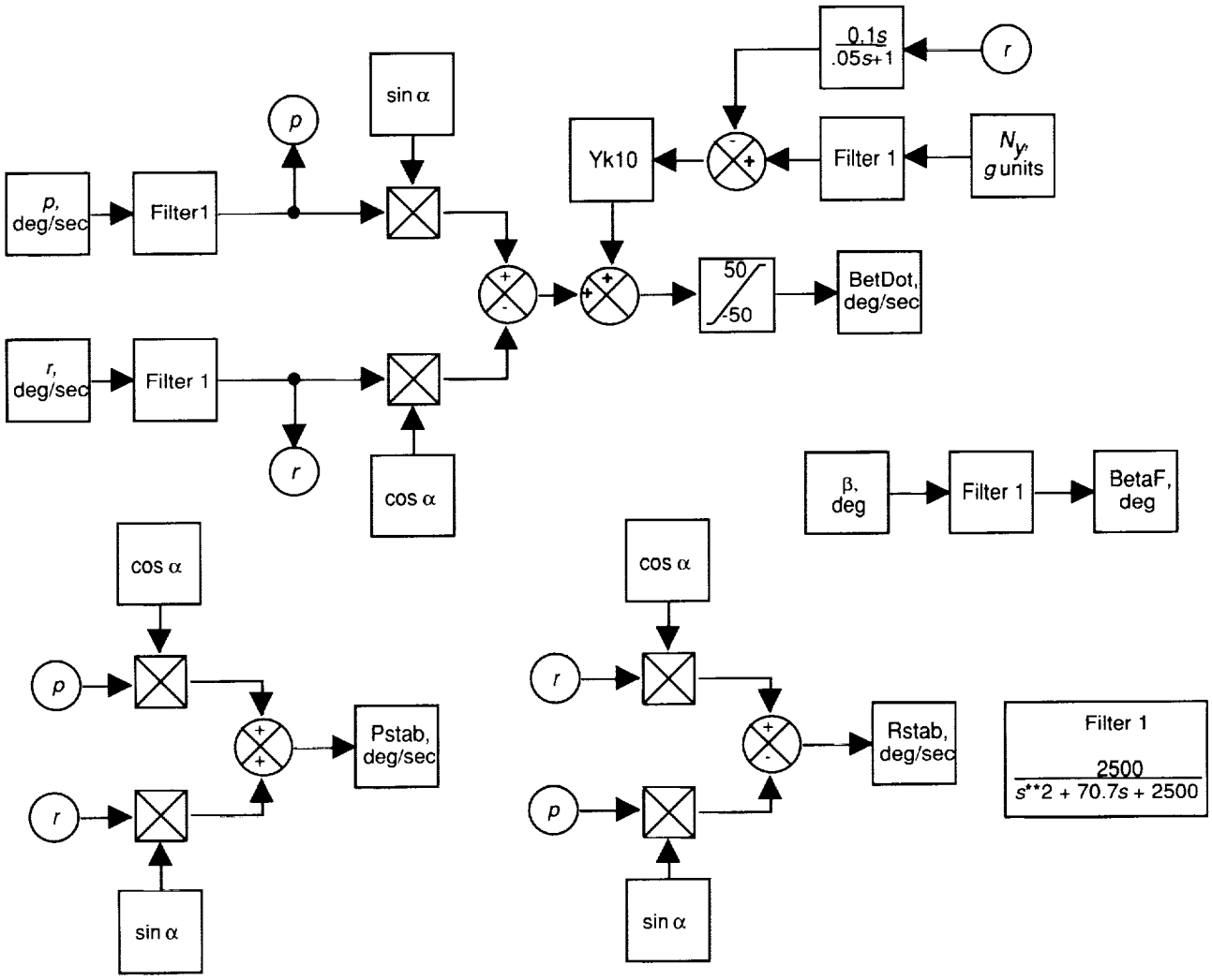

(e) Lateral-directional feedback signals.

Figure 8. Concluded.

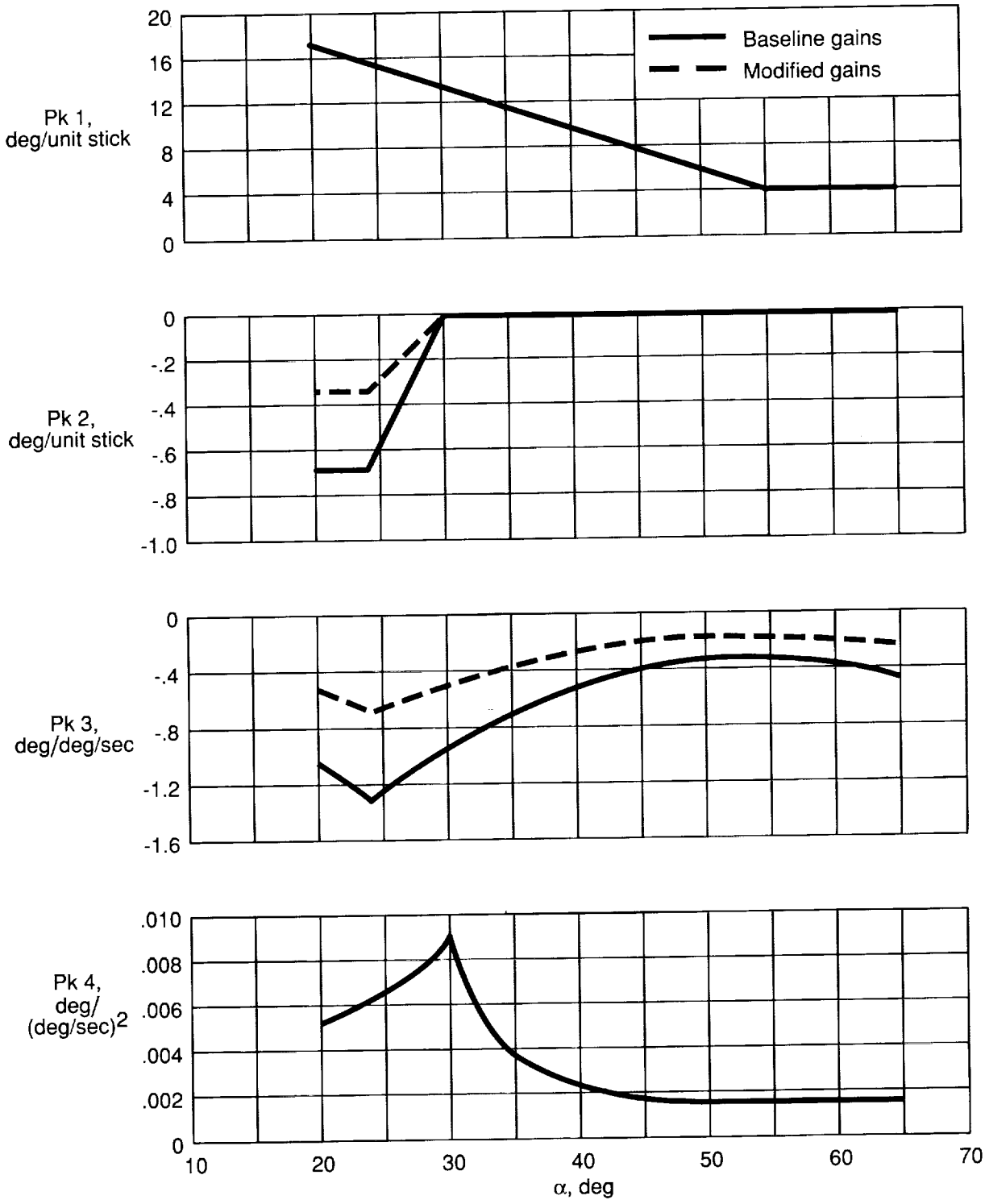

Figure 9. Free-flight feedback gain schedules.

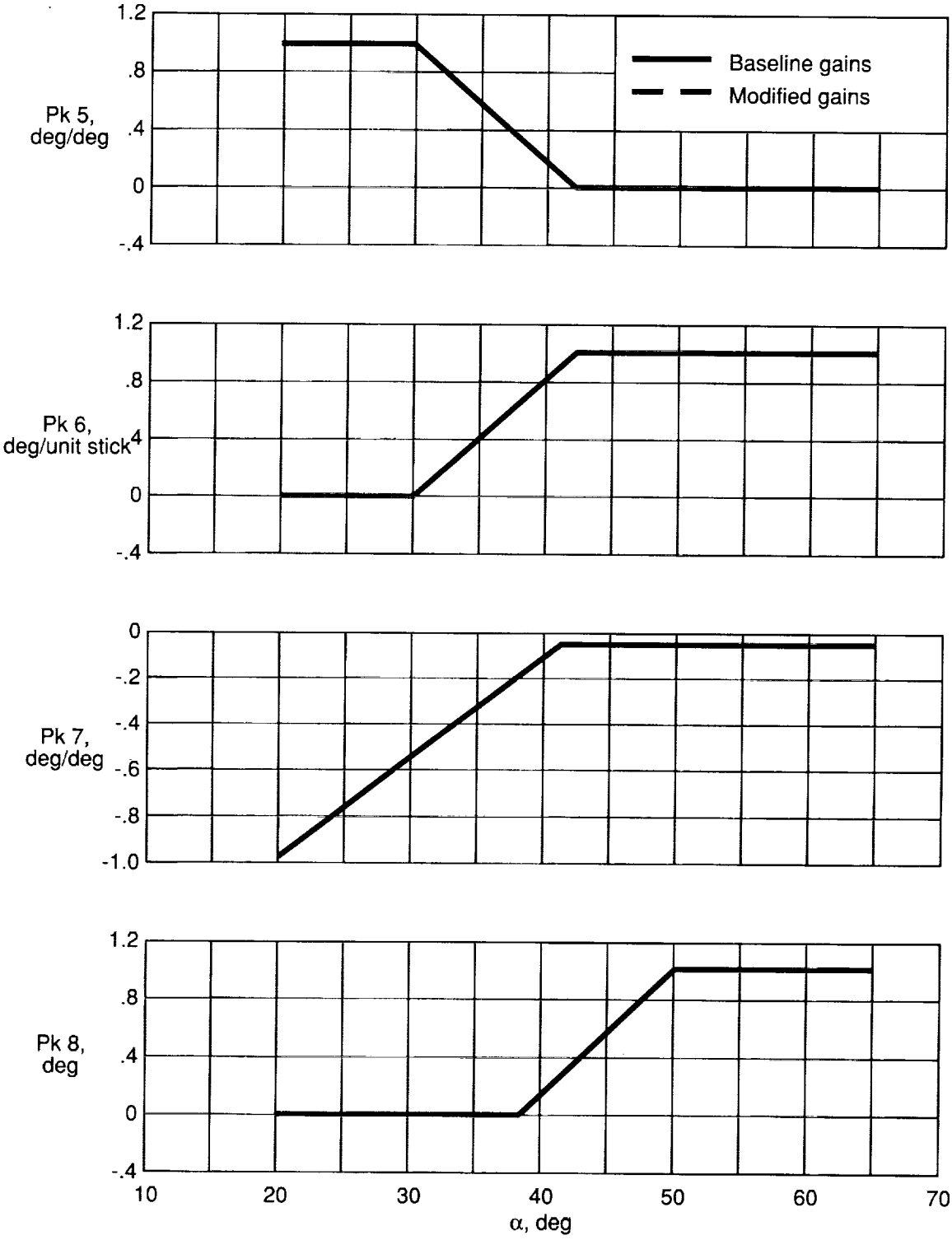

Figure 9. Continued.

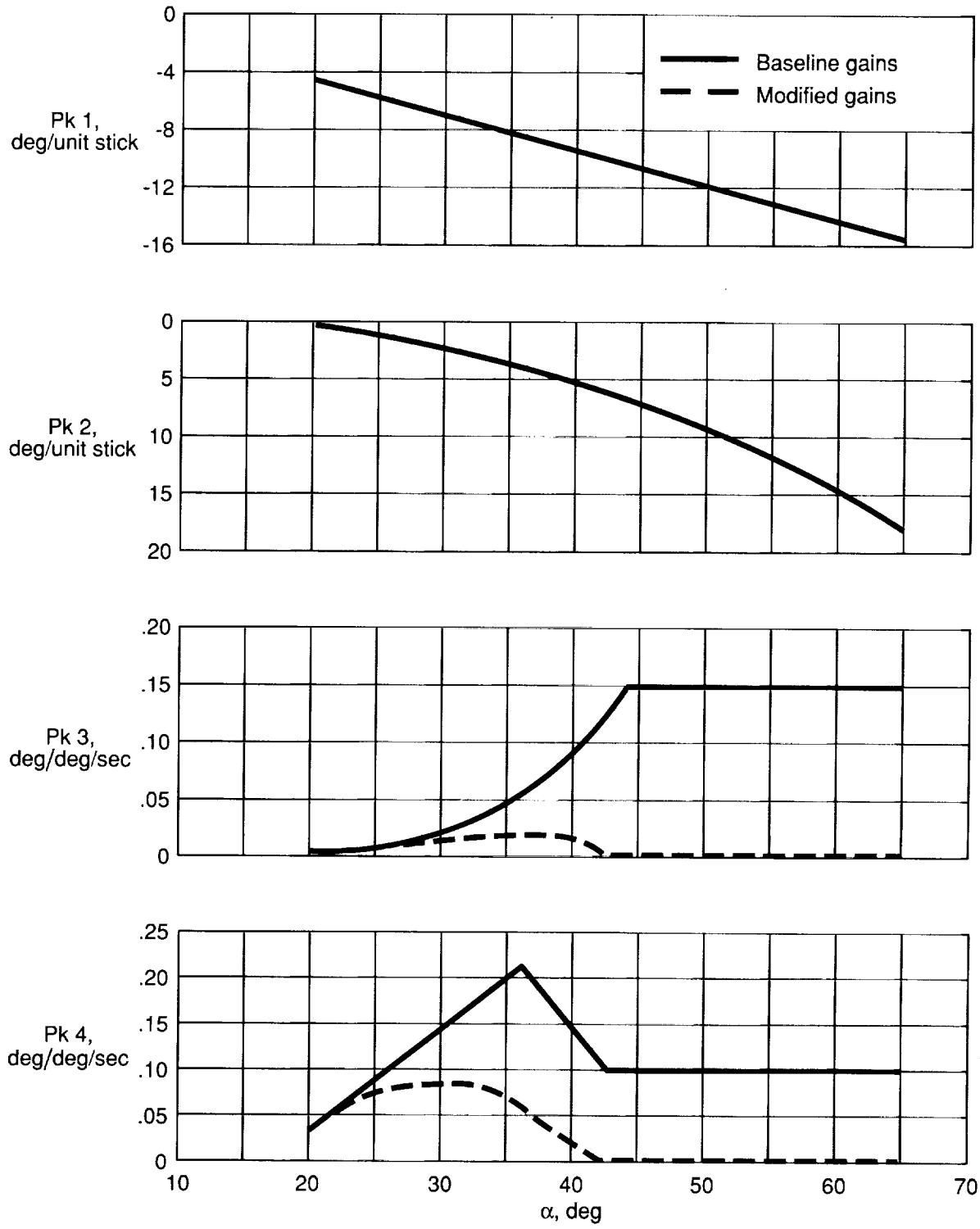

Figure 9. Continued.

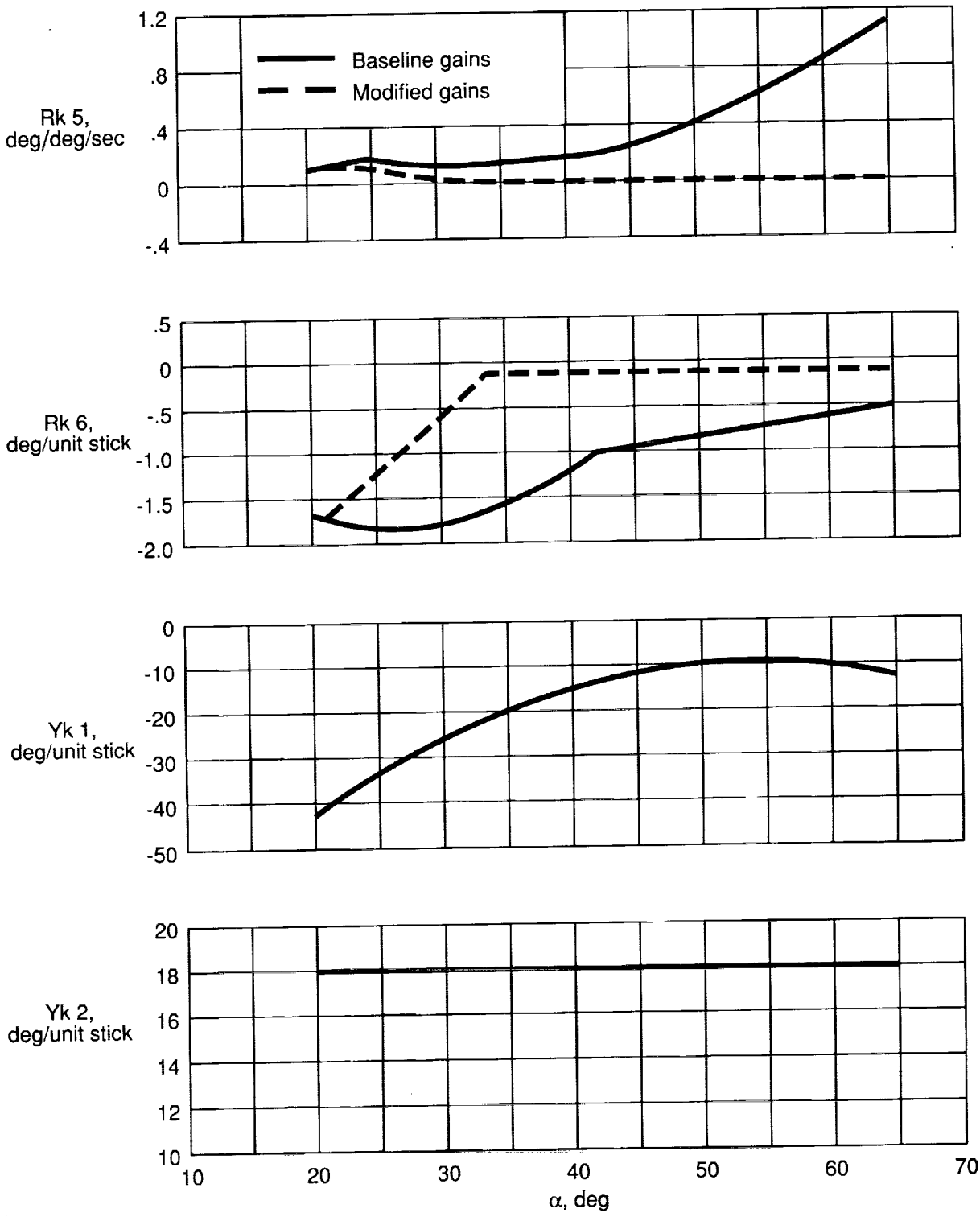

Figure 9. Continued.

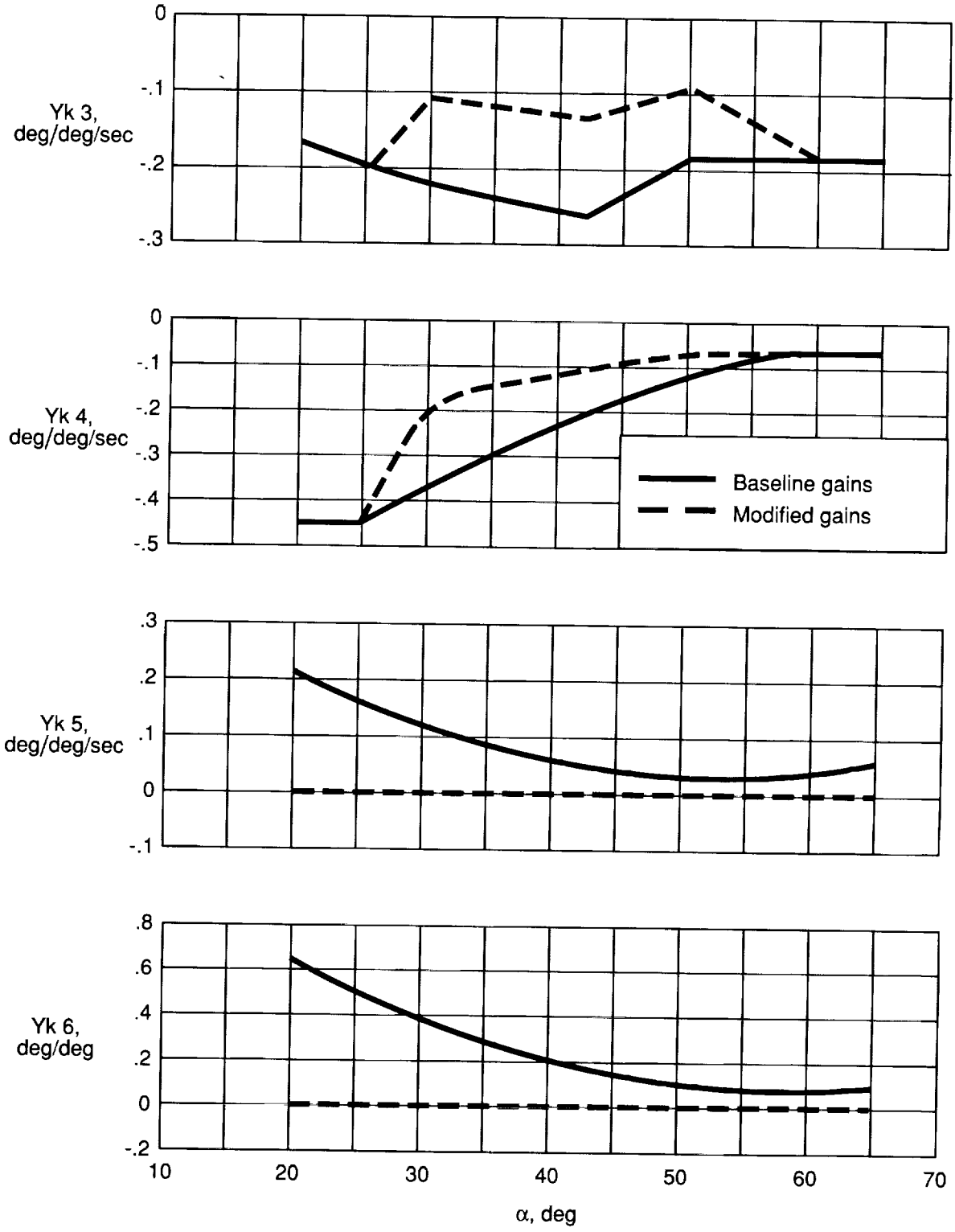

Figure 9. Continued.

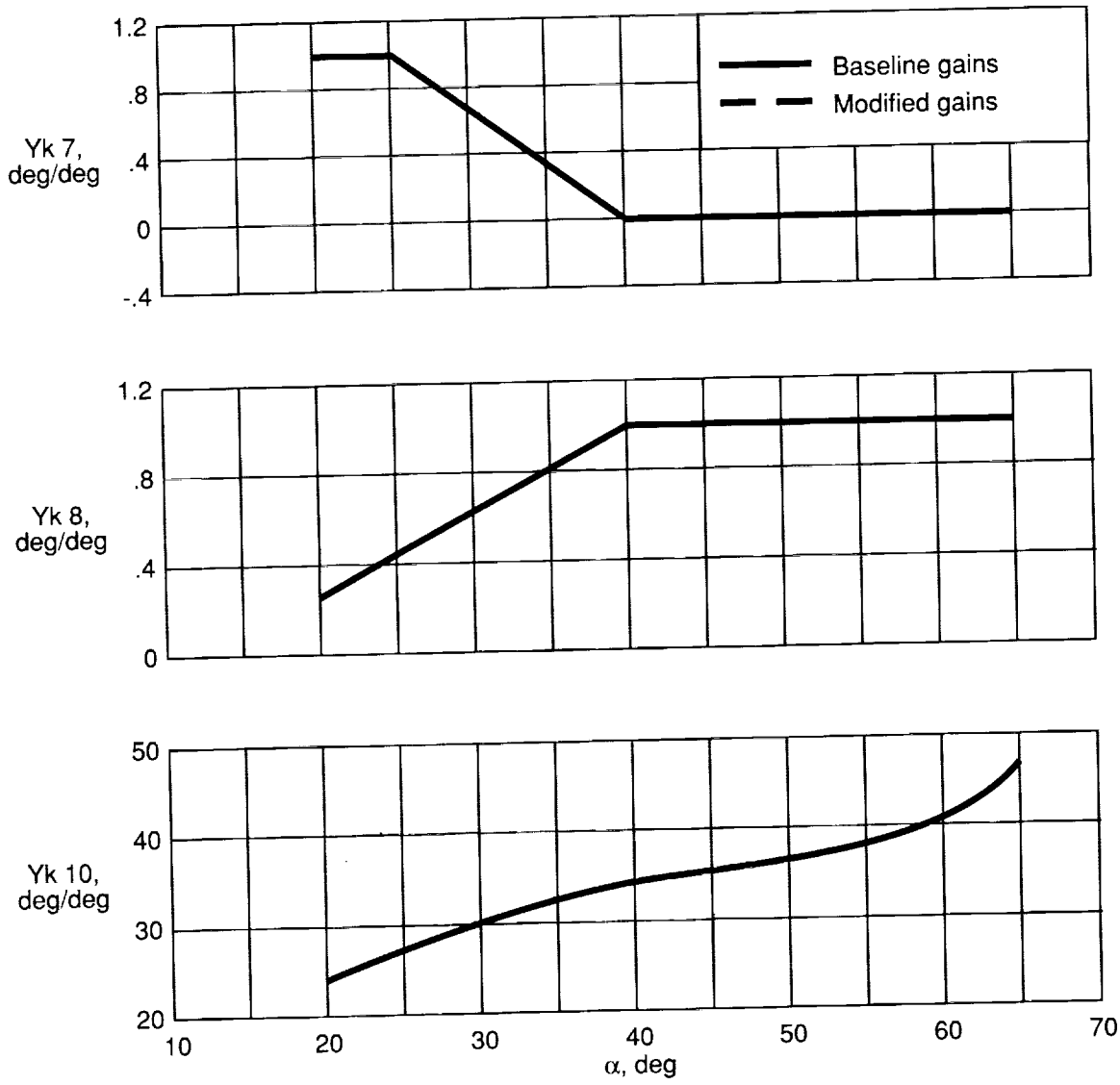

Figure 9. Concluded.

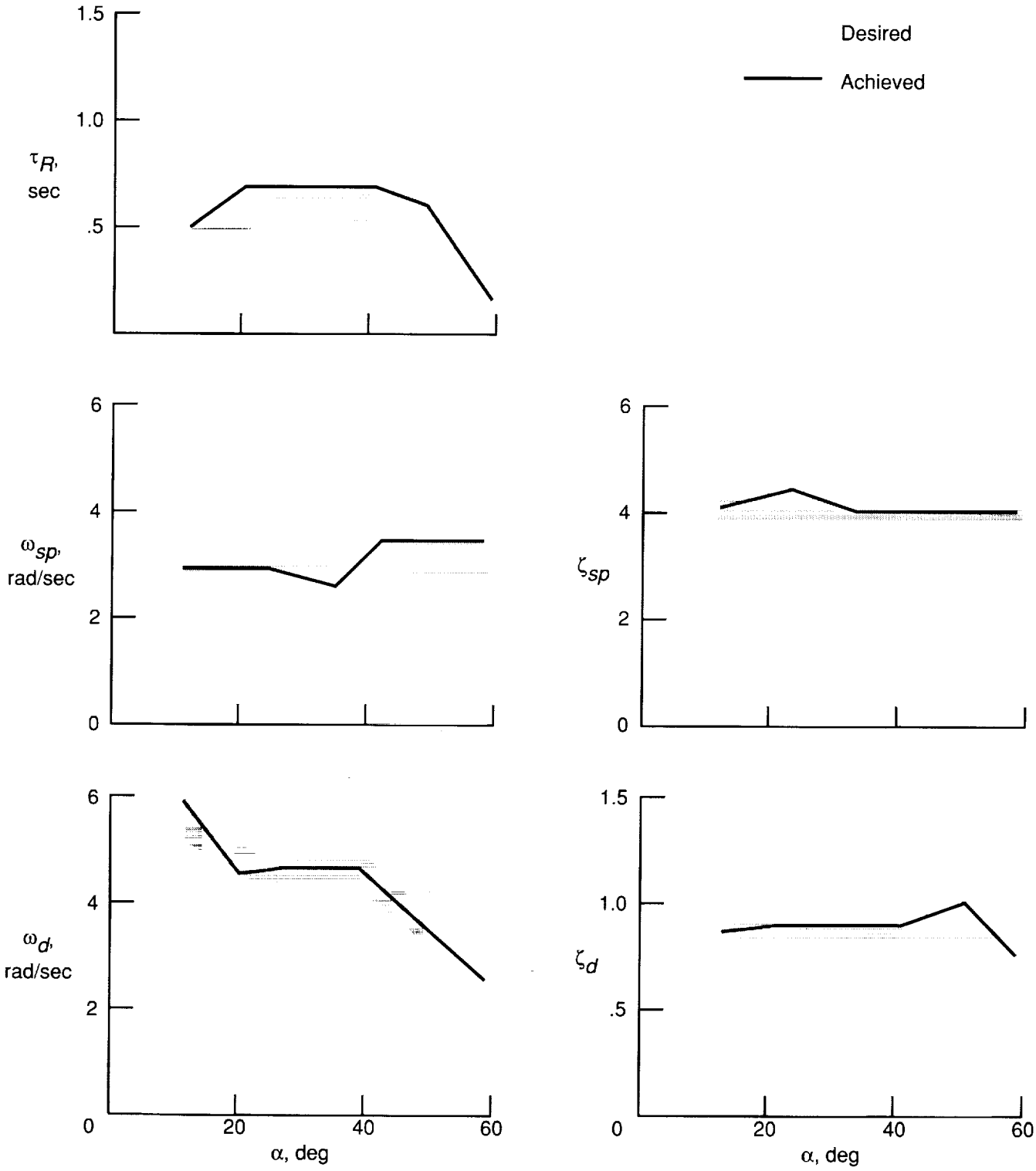

Figure 10. Linear evaluation of control system.

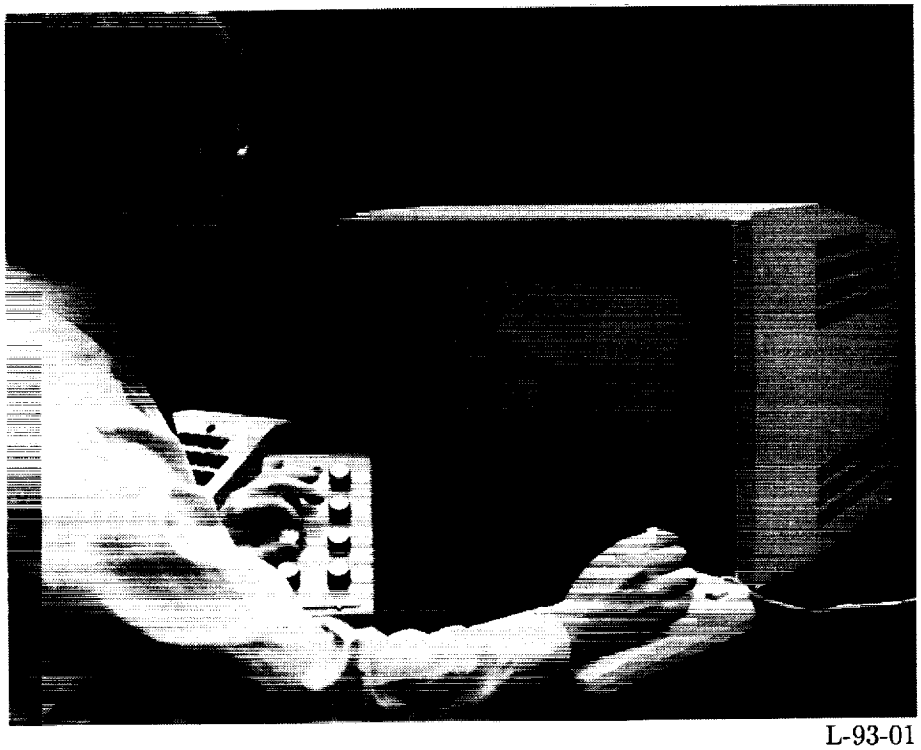

L-93-01

(a) Pilot at work station.

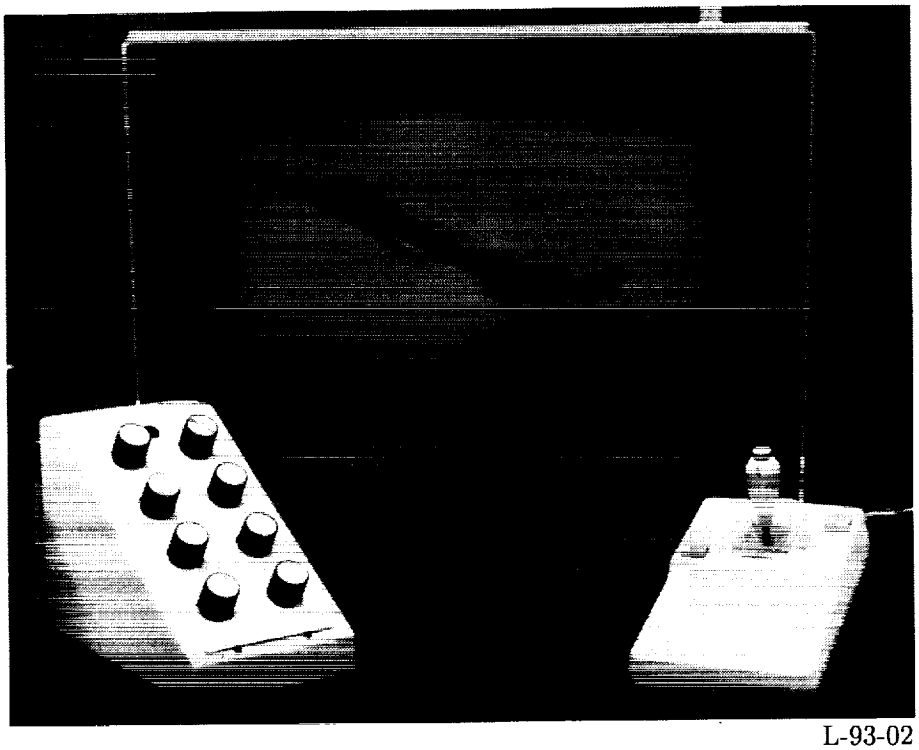

L-93-02

(b) Close-up of work station.

Figure 11. Real-time-engineering simulation work station.

ORIGINAL PAGE
BLACK AND WHITE PHOTOGRAPH

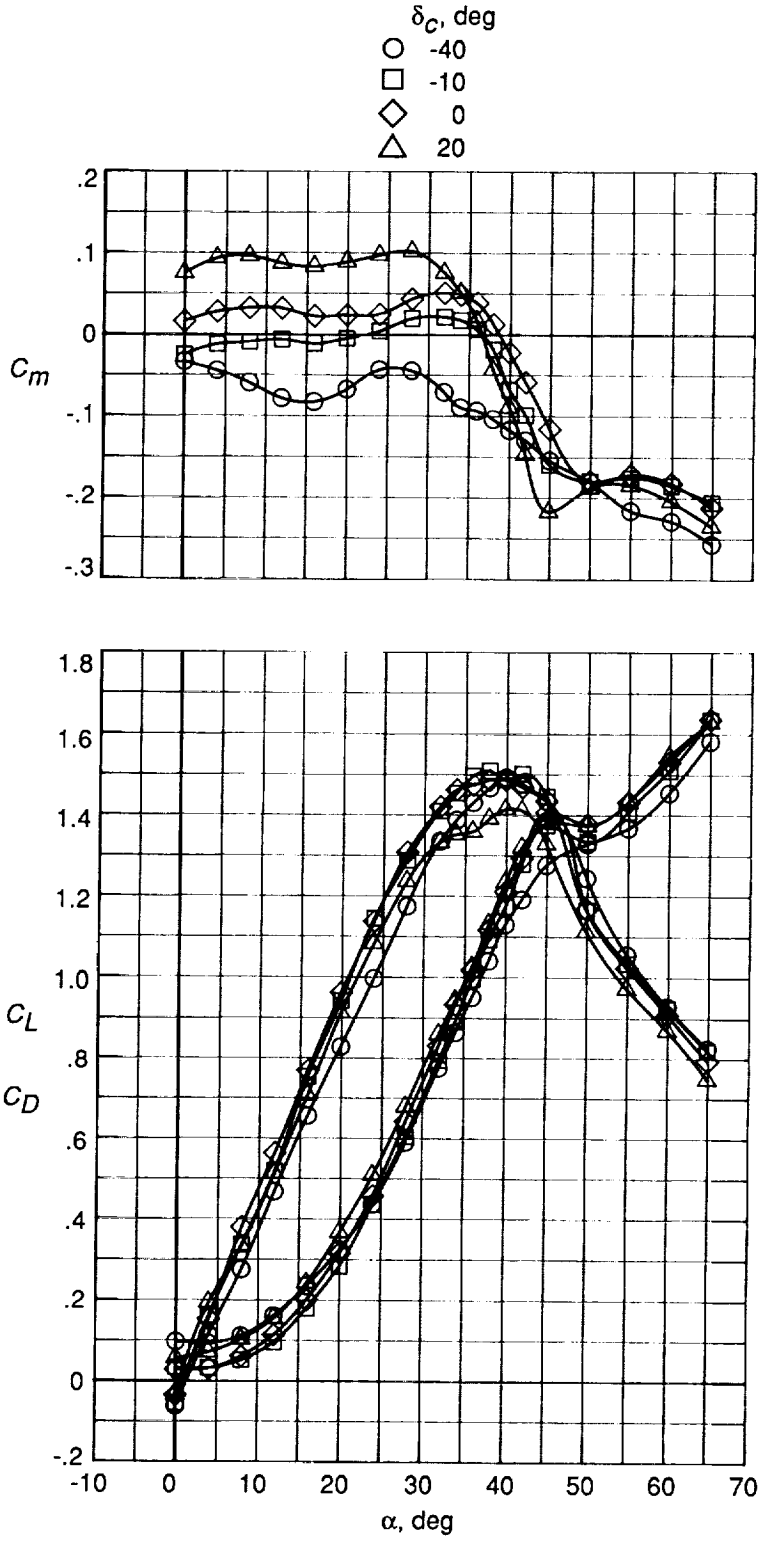

Figure 12. Effect of canard deflection on longitudinal characteristics. $\delta_f = 30°$; $\delta_F = 0°$.

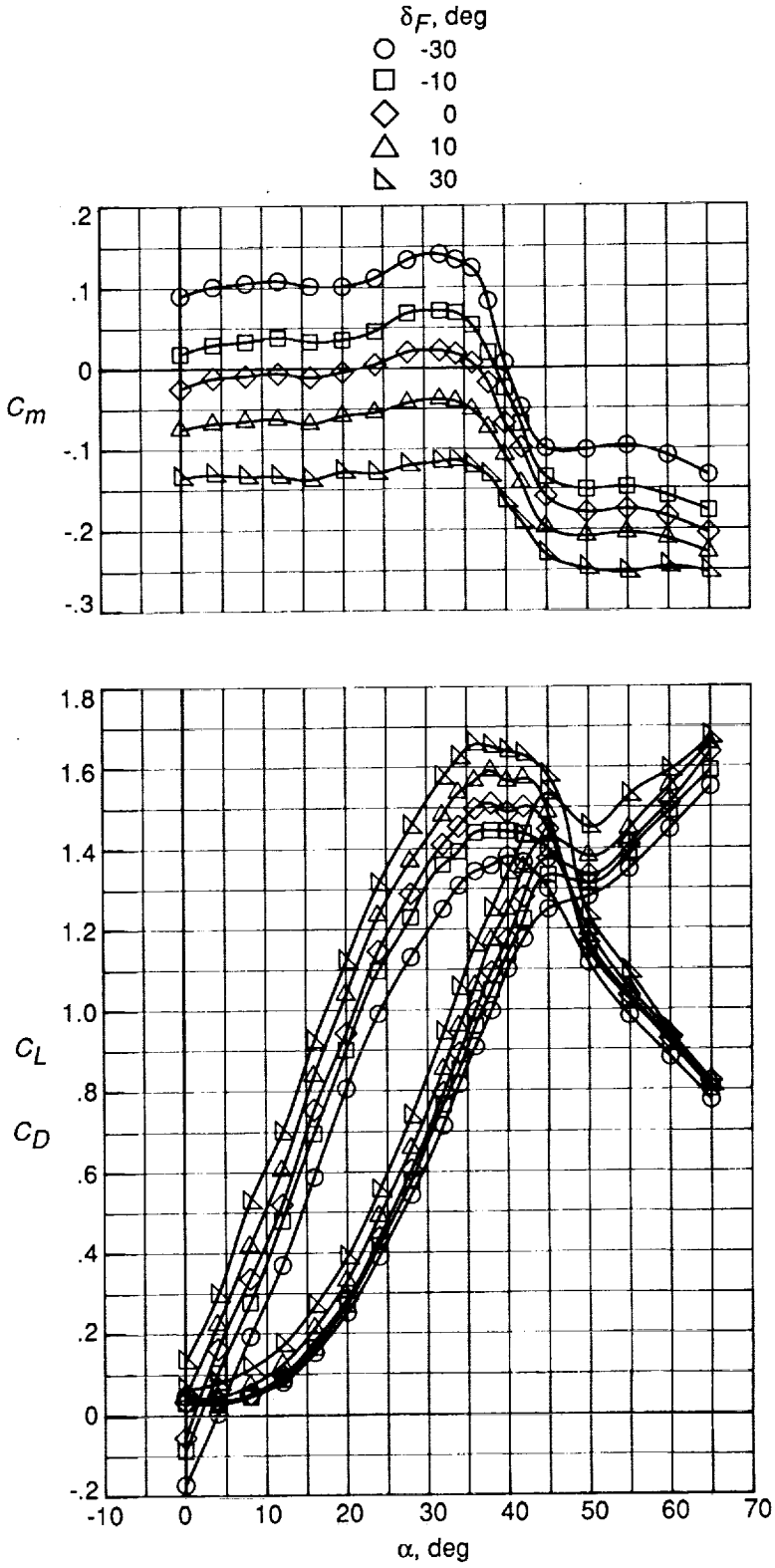

Figure 13. Effect of TEX flap deflection on longitudinal characteristics. $\delta_f = 30°$; $\delta_c = -10°$.

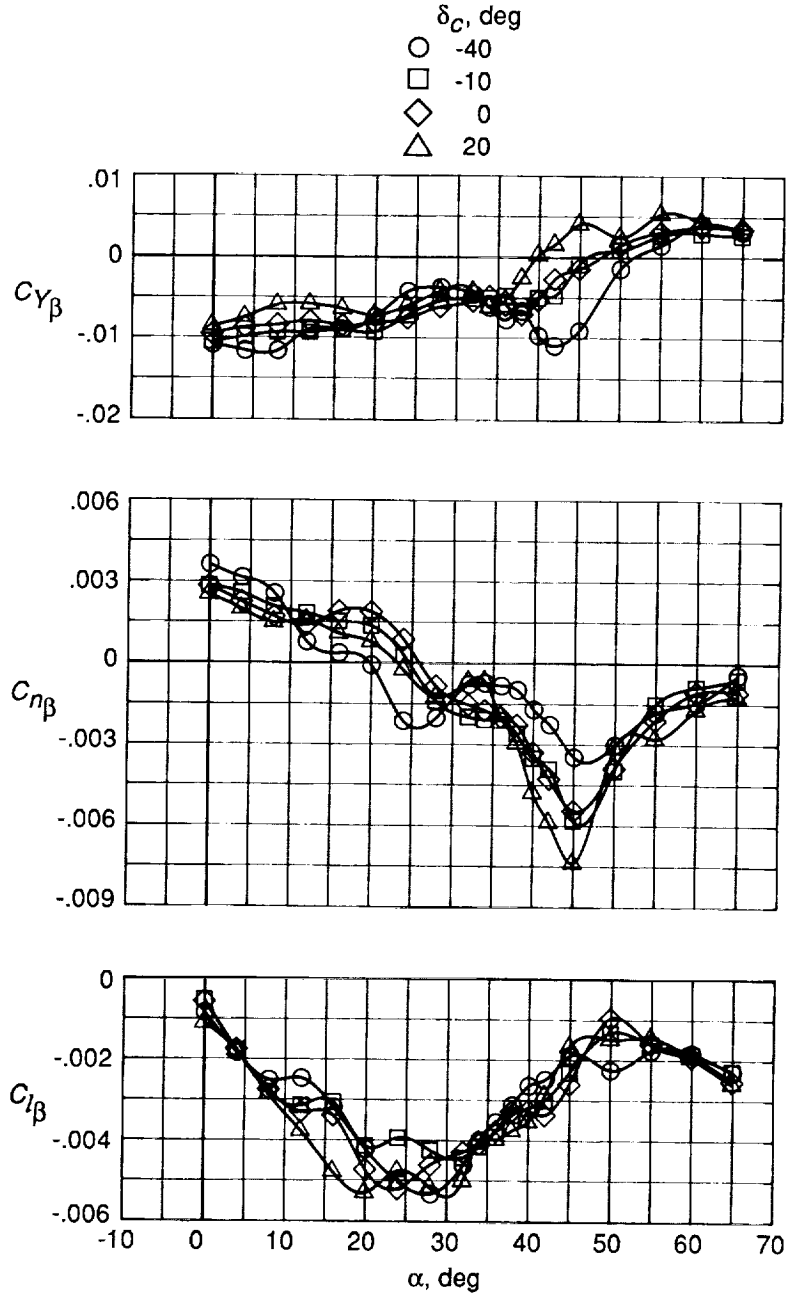

Figure 14. Effect of canard deflection on lateral-directional characteristics. $\delta_f = 30°$; $\delta_F = 0°$.

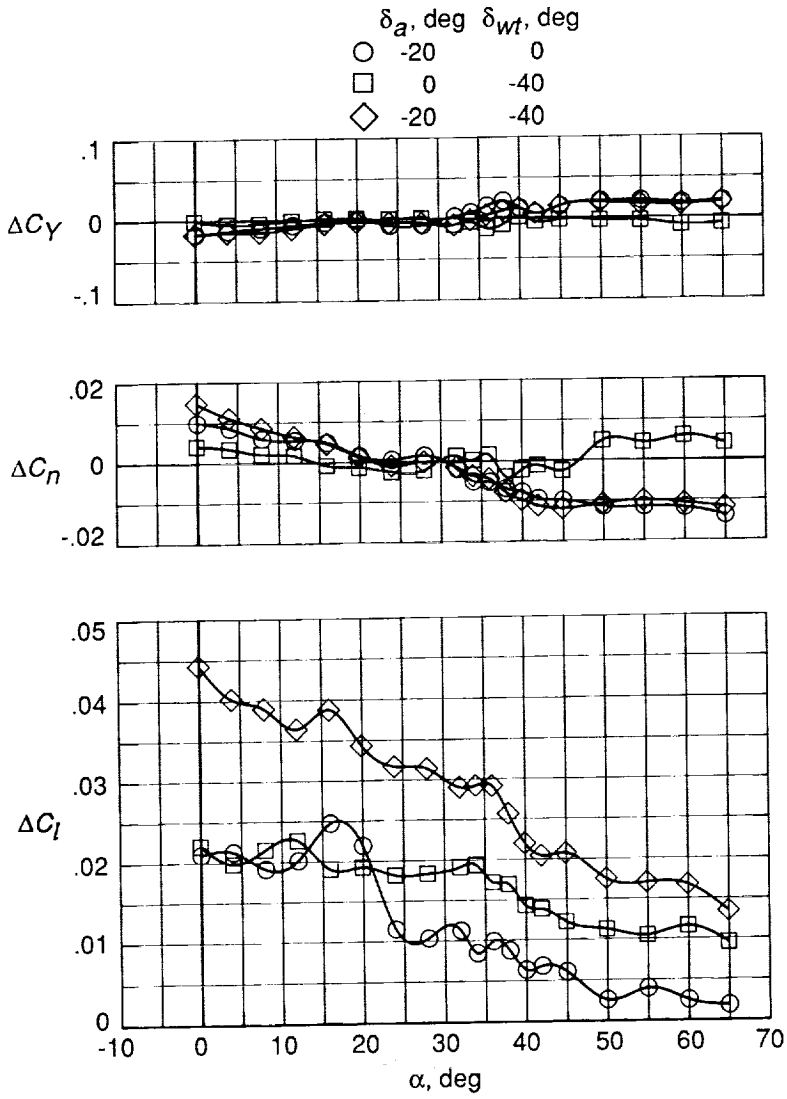

(a) Combined aileron and tiperon control effectiveness. $\delta_f = 30°$; $\delta_c = -10°$; $\delta_F = 0°$.

Figure 15. Lateral-directional control effectiveness.

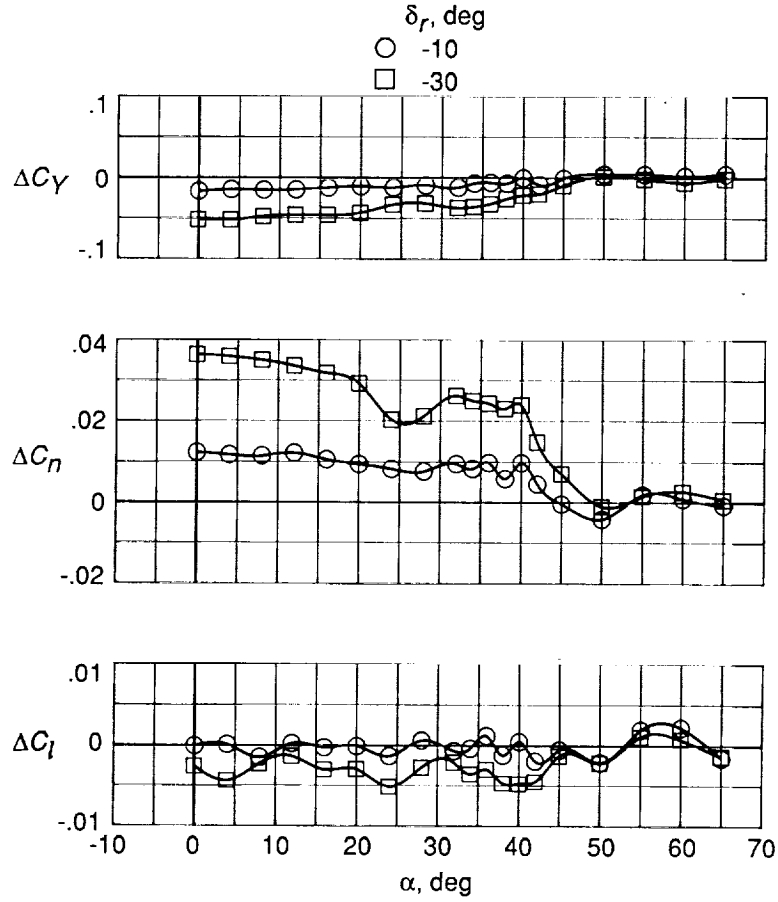

(b) Rudder control effectiveness. $\delta_f = 30°$; $\delta_c = -10°$; $\delta_F = 0°$.

Figure 15. Concluded.

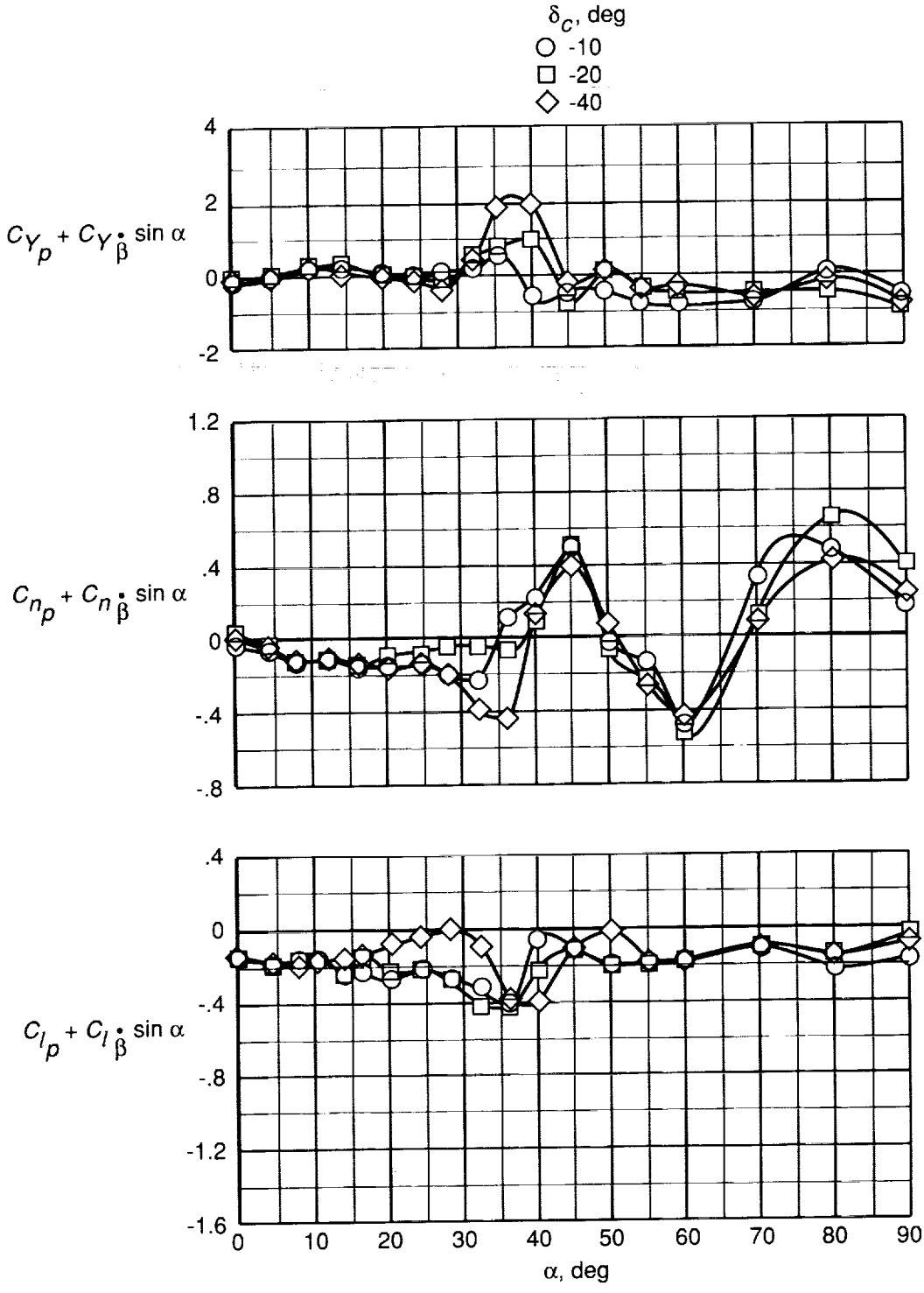

Figure 16. Effect of canard deflection on roll damping. $\delta_f = 30°$; $\delta_F = 0°$.

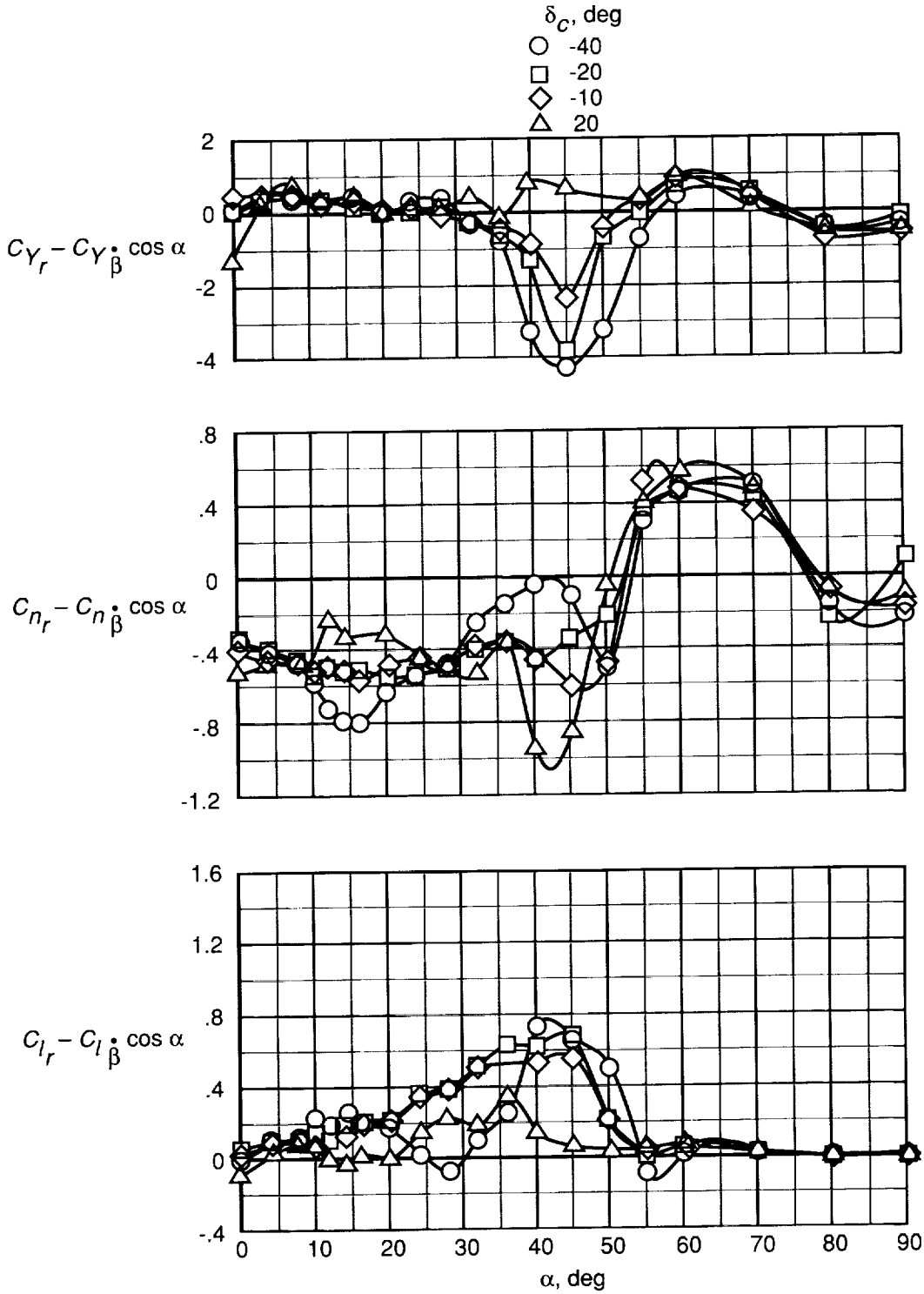

Figure 17. Effect of canard deflection on yaw damping. $\delta_f = 30°$; $\delta_F = 0°$.

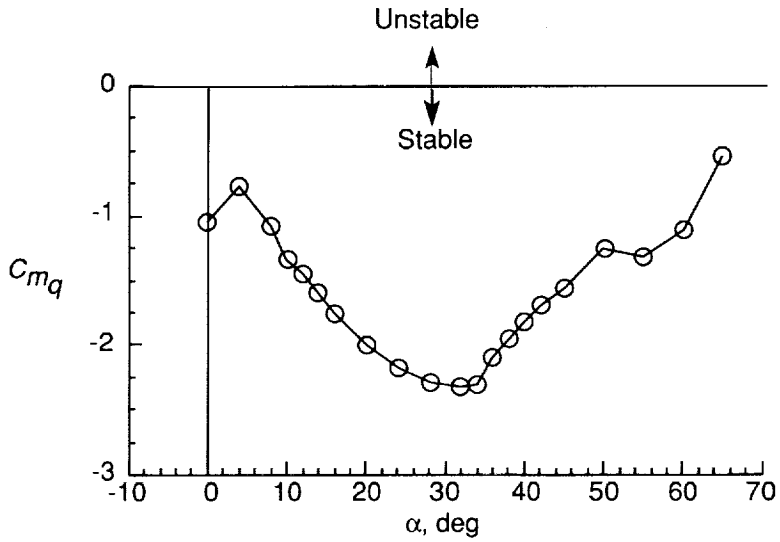

Figure 18. Estimated pitch-damping characteristics.

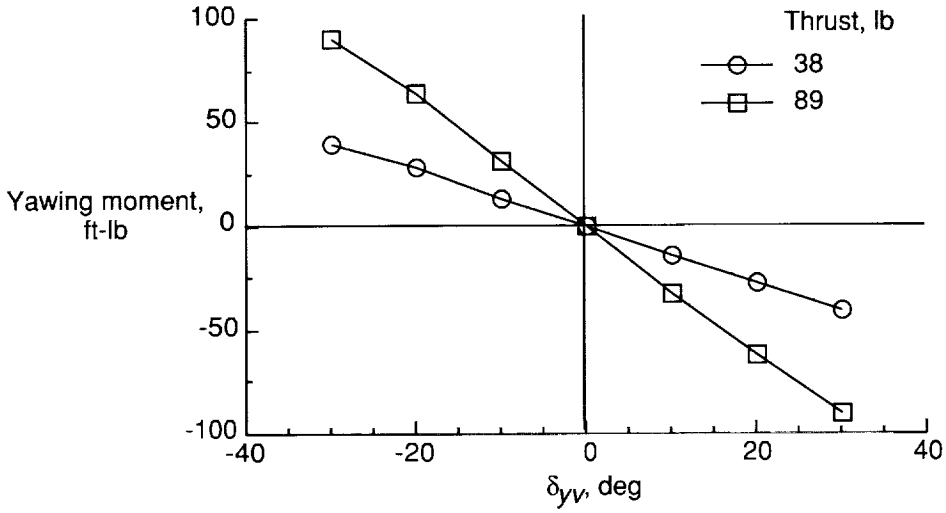

(a) Yaw vectoring.

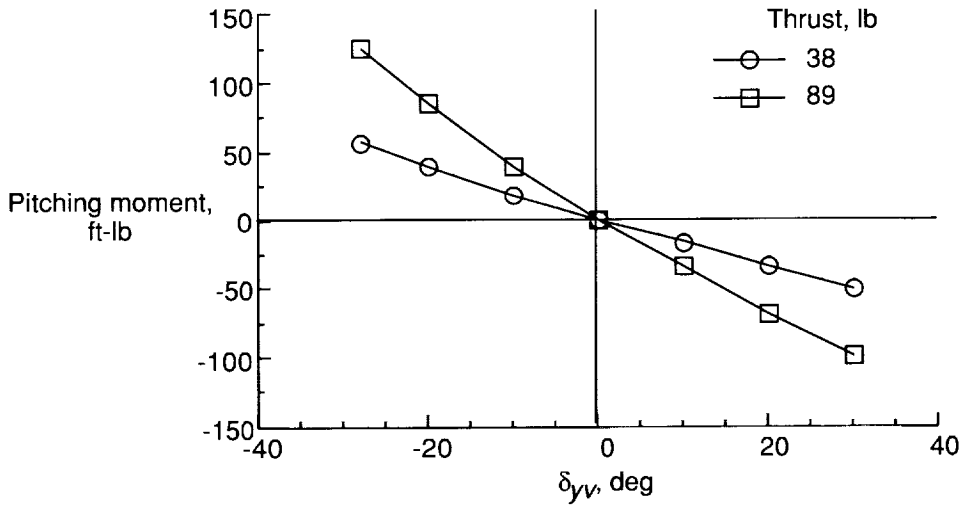

(b) Pitch vectoring.

Figure 19. Wind-off thrust-vectoring effectiveness.

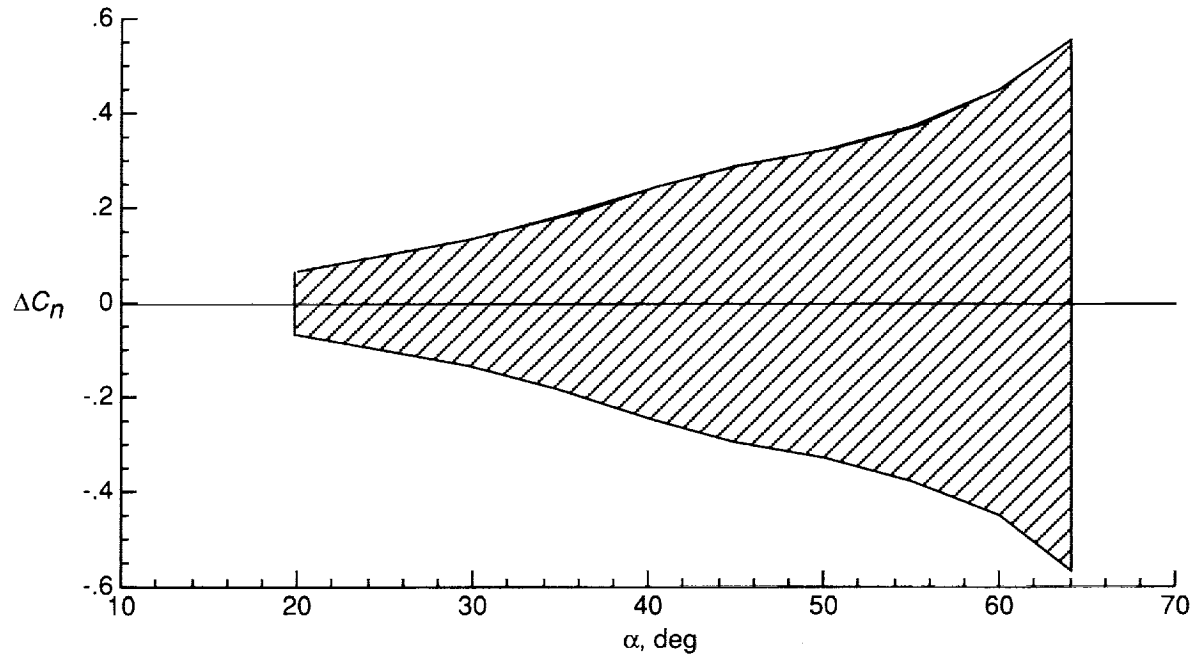

(a) Yaw vectoring.

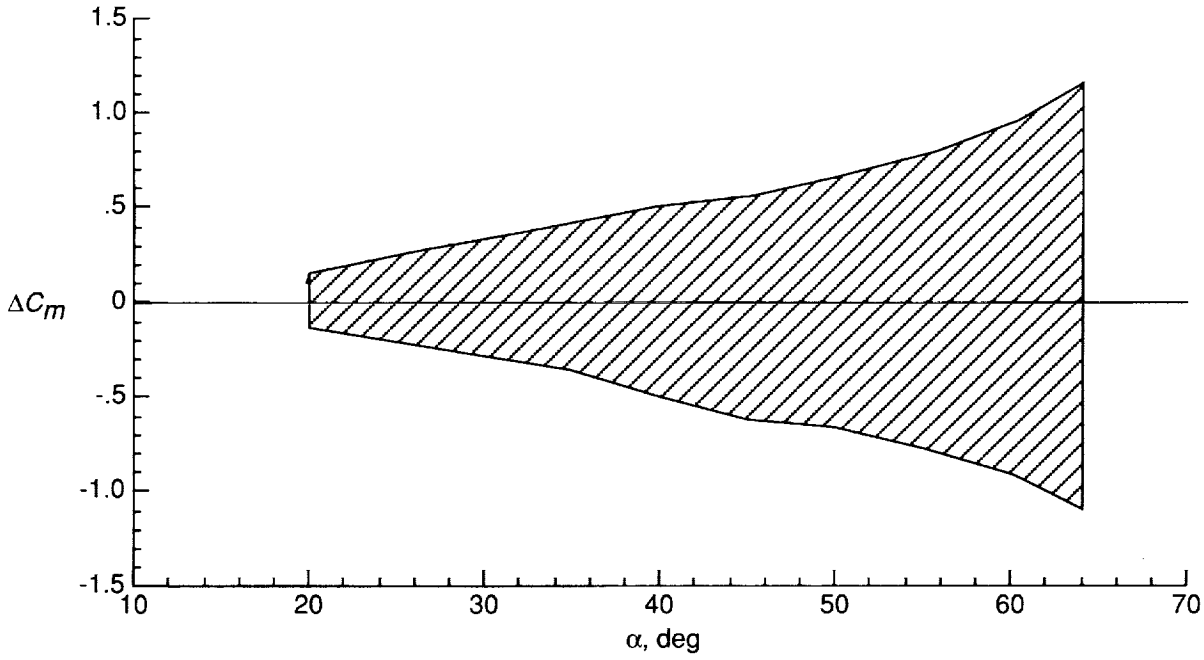

(b) Pitch vectoring.

Figure 20. Thrust-vectoring effectiveness for estimated trimmed flight conditions.

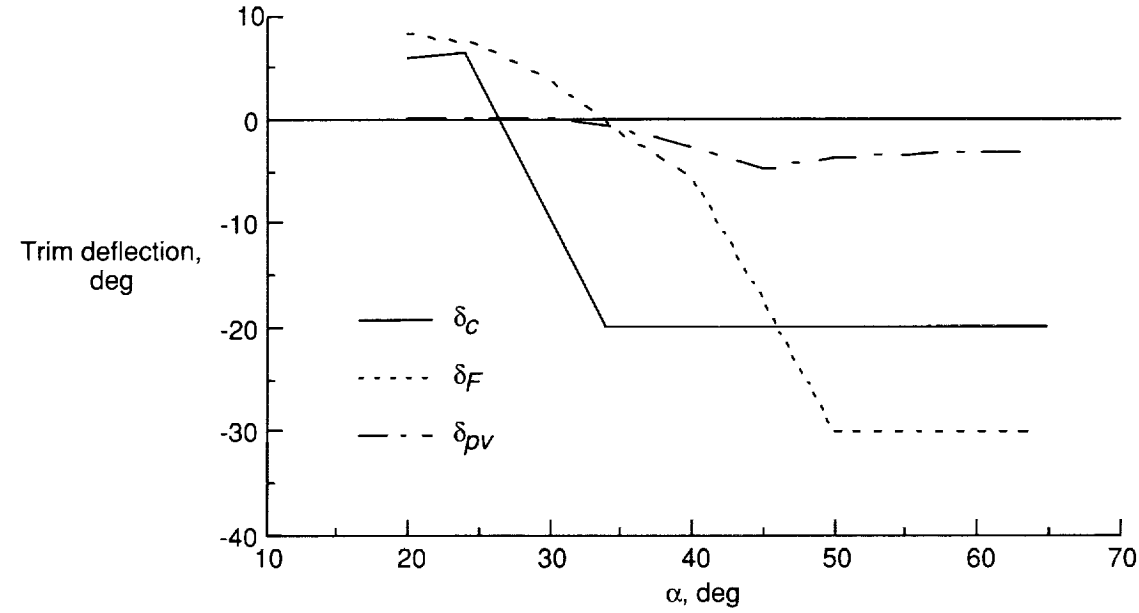

(a) Trim control settings.

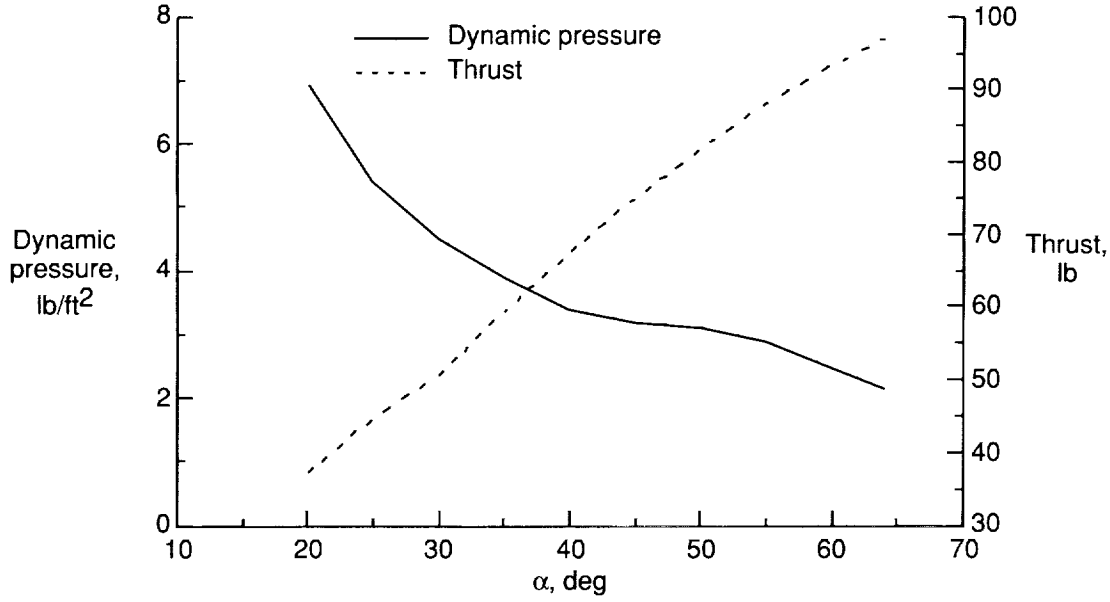

(b) Trim dynamic pressure and thrust.

Figure 21. Predicted trim controls, dynamic pressure, and thrust of free-flight model.

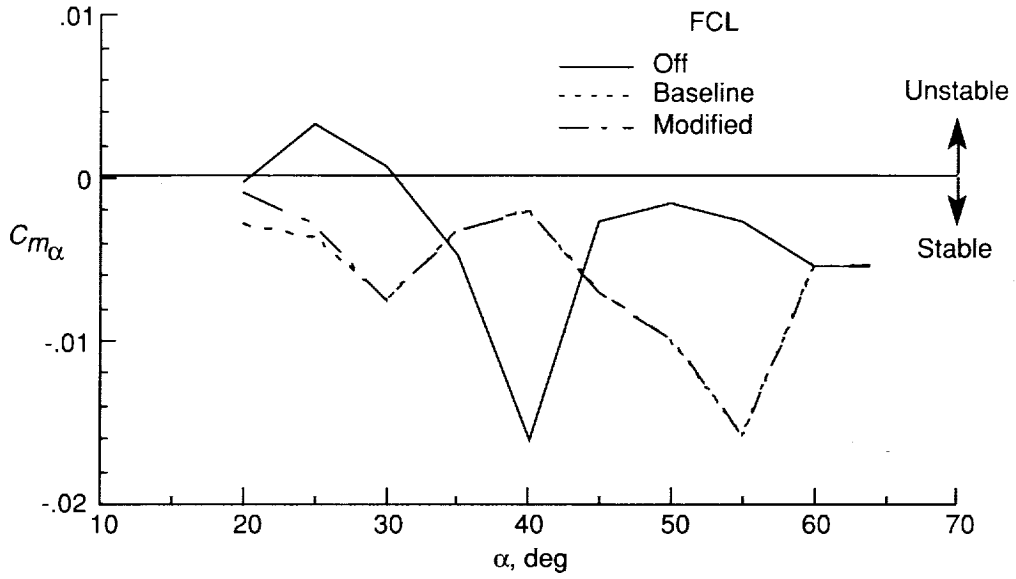

(a) Static pitch stability.

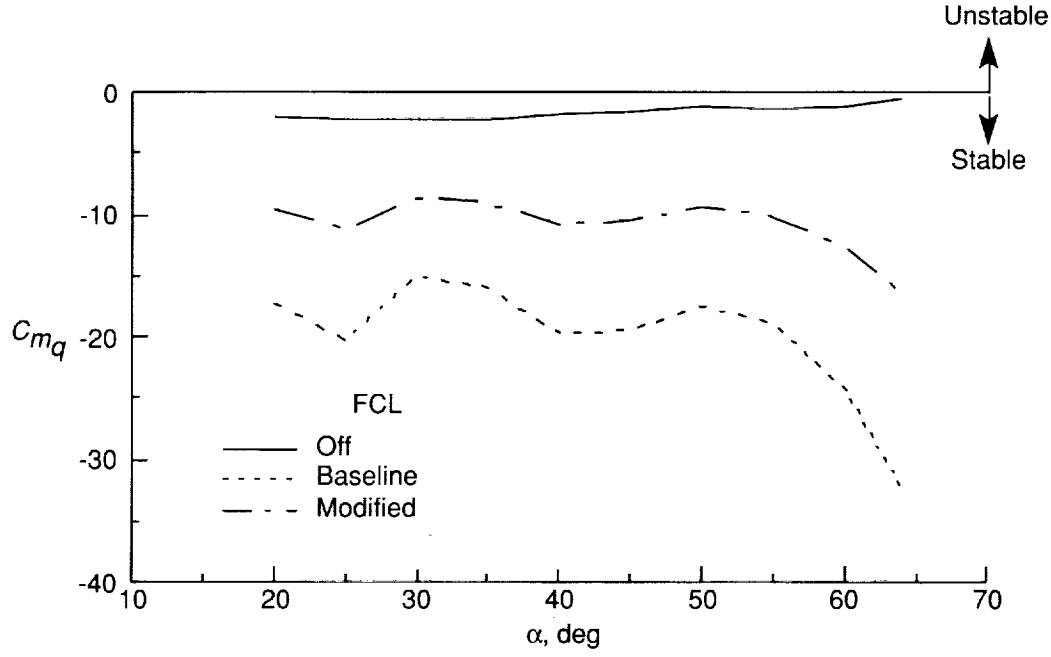

(b) Dynamic pitch stability.

Figure 22. Longitudinal stability characteristics of free-flight model for trimmed flight.

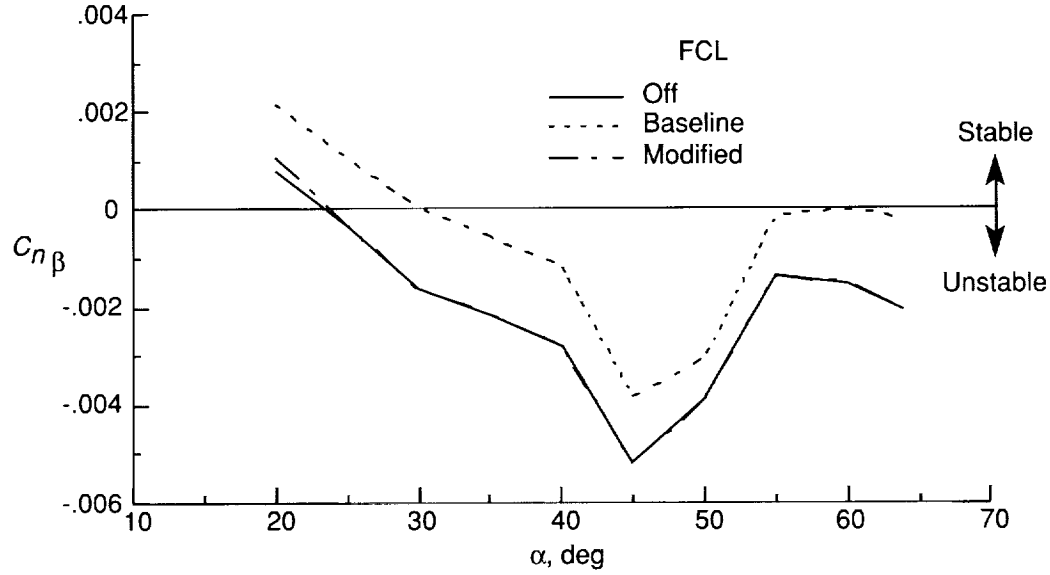

(a) Directional stability.

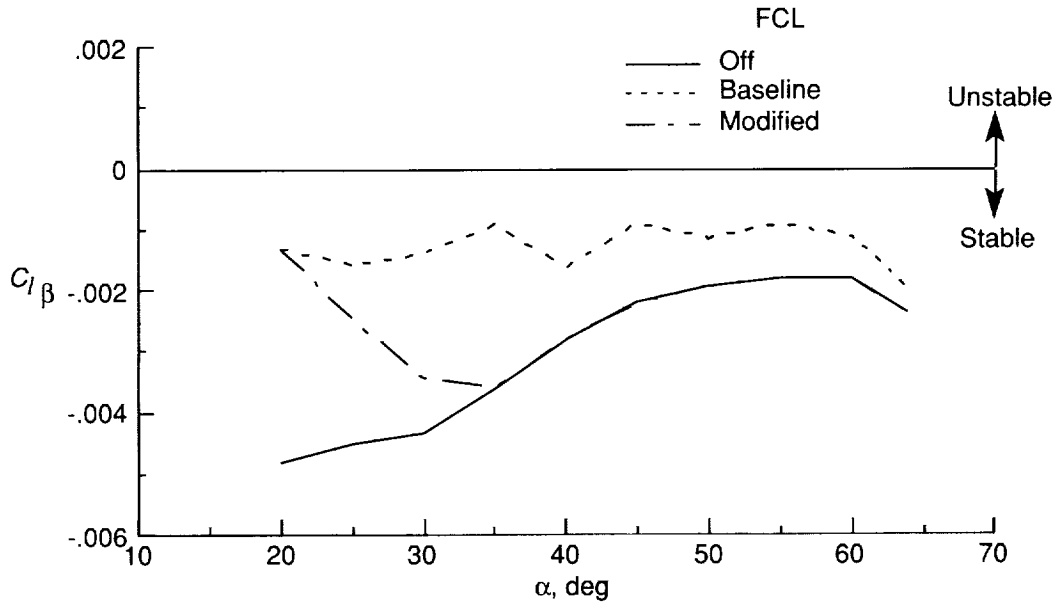

(b) Lateral stability.

Figure 23. Static lateral-directional stability characteristics of free-flight model for trimmed flight.

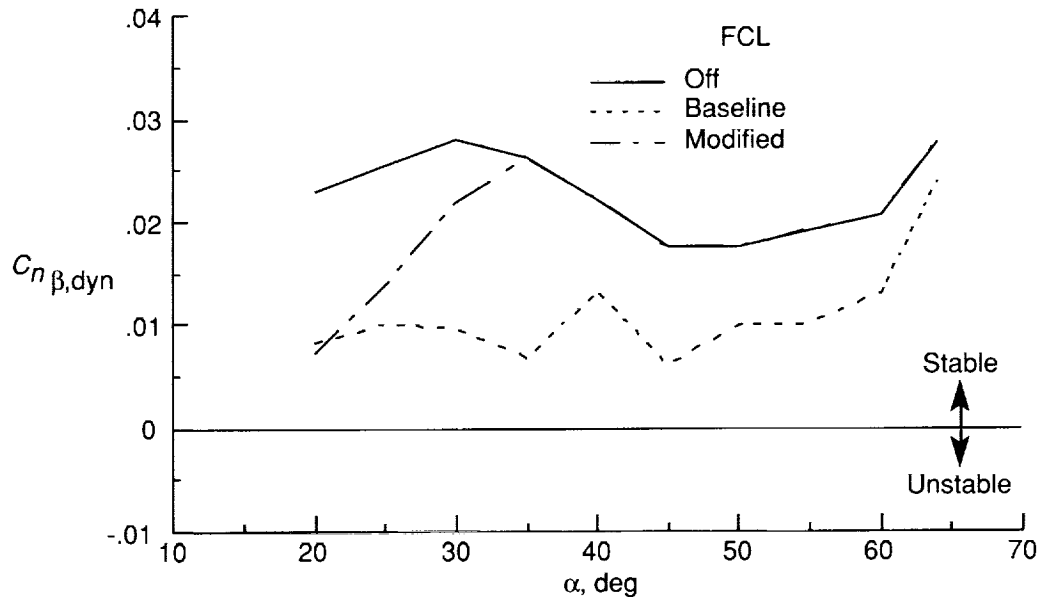

Figure 24. Yaw divergence resistance of the free-flight model for trimmed flight.

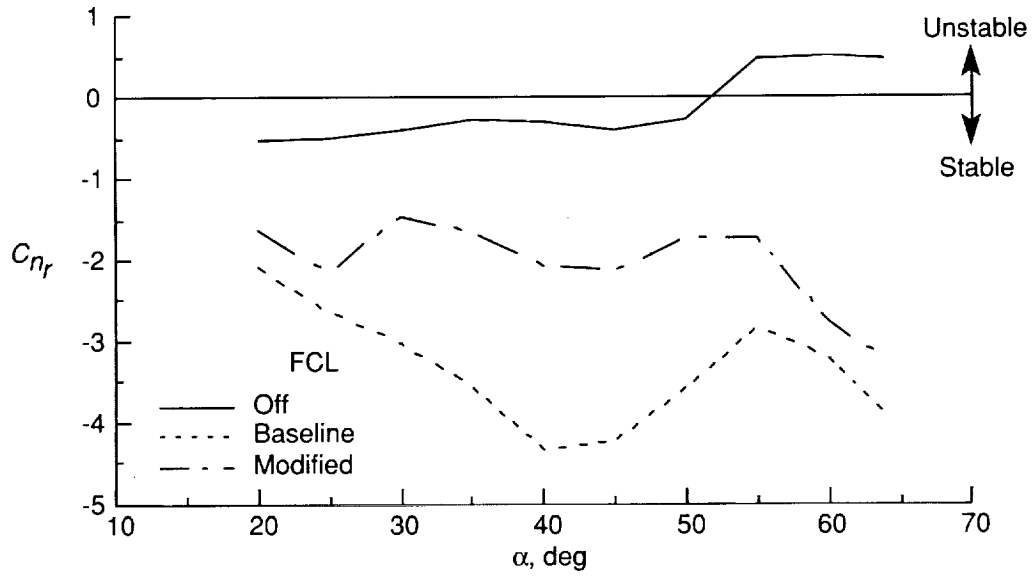

(a) Yaw-damping characteristics.

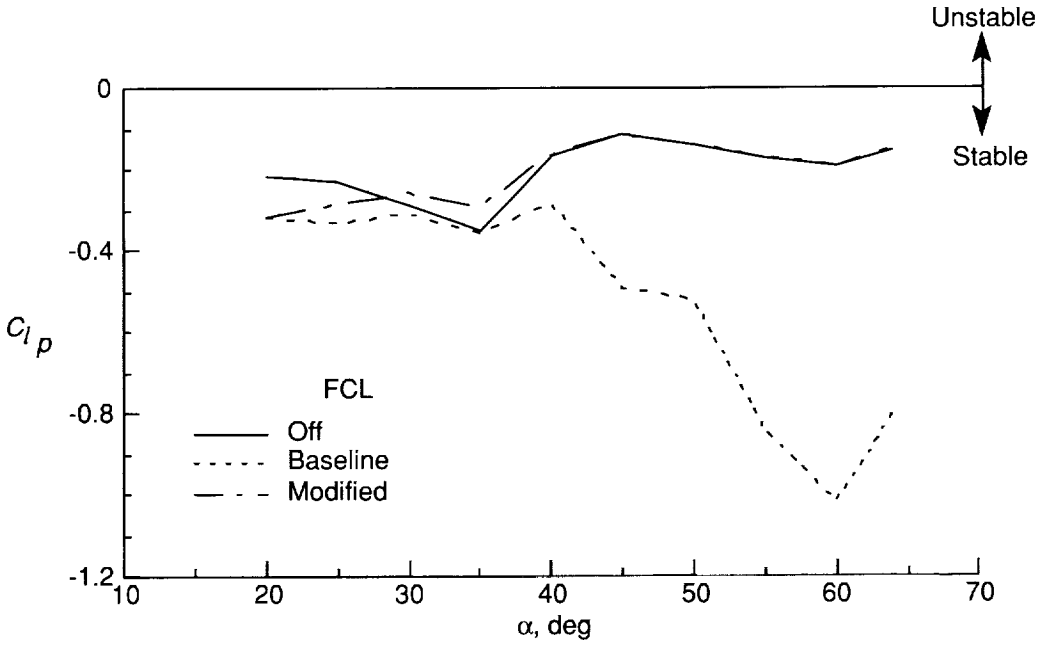

(b) Roll-damping characteristics.

Figure 25. Lateral-directional damping characteristics of free-flight model for trimmed flight.

REPORT DOCUMENTATION PAGE

Form Approved
OMB No. 0704-0188

Public reporting burden for this collection of information is estimated to average 1 hour per response, including the time for reviewing instructions, searching existing data sources, gathering and maintaining the data needed, and completing and reviewing the collection of information. Send comments regarding this burden estimate or any other aspect of this collection of information, including suggestions for reducing this burden, to Washington Headquarters Services, Directorate for Information Operations and Reports, 1215 Jefferson Davis Highway, Suite 1204, Arlington, VA 22202-4302, and to the Office of Management and Budget, Paperwork Reduction Project (0704-0188), Washington, DC 20503.

1. AGENCY USE ONLY *(Leave blank)*	2. REPORT DATE	3. REPORT TYPE AND DATES COVERED
	February 1993	Technical Paper

4. TITLE AND SUBTITLE
Wind-Tunnel Free-Flight Investigation of a Supersonic Persistence Fighter

5. FUNDING NUMBERS
WU 505-59-30-07

6. AUTHOR(S)
David E. Hahne, Thomas R. Wendel, and Joseph R. Boland

7. PERFORMING ORGANIZATION NAME(S) AND ADDRESS(ES)
NASA Langley Research Center
Hampton, VA 23681-0001

8. PERFORMING ORGANIZATION REPORT NUMBER
L-17040

9. SPONSORING/MONITORING AGENCY NAME(S) AND ADDRESS(ES)
National Aeronautics and Space Administration
Washington, DC 20546-0001

10. SPONSORING/MONITORING AGENCY REPORT NUMBER
NASA TP-3258

11. SUPPLEMENTARY NOTES
Hahne: Langley Research Center, Hampton, VA; Wendel and Boland: McDonnell Aircraft Company, St. Louis, MO.

12a. DISTRIBUTION/AVAILABILITY STATEMENT
Unclassified–Unlimited

Subject Categories 02 and 08

12b. DISTRIBUTION CODE

13. ABSTRACT *(Maximum 200 words)*
Wind-tunnel free-flight tests have been conducted in the Langley 30- by 60-Foot Tunnel to examine the high-angle-of-attack stability and control characteristics and control law design of a supersonic persistence fighter (SSPF) at 1g flight conditions. In addition to conventional control surfaces, the SSPF incorporated deflectable wingtips (tiperons) and pitch and yaw thrust vectoring. A direct eigenstructure assignment technique was used to design control laws to provide good flying characteristics well into the poststall angle-of-attack region. Free-flight tests indicated that it was possible to blend effectively conventional and unconventional control surfaces to achieve good flying characteristics well into the poststall angle-of-attack region.

14. SUBJECT TERMS
Control law design; Advanced fighter; Free flight; Dynamic stability

15. NUMBER OF PAGES
60

16. PRICE CODE
A04

17. SECURITY CLASSIFICATION OF REPORT	18. SECURITY CLASSIFICATION OF THIS PAGE	19. SECURITY CLASSIFICATION OF ABSTRACT	20. LIMITATION OF ABSTRACT
Unclassified	Unclassified		

NSN 7540-01-280-5500

Standard Form 298(Rev. 2-89)
Prescribed by ANSI Std. Z39-18
298-102

NASA-Langley, 1993